Quaternary Science Reviews 375 (2026) 109769

Contents lists available at ScienceDirect

Quaternary Science Reviews

journal homepage: www.elsevier.com/locate/quascirev

# Last interglacial relative sea-level changes at Myrtle Beach, South Carolina

S. Dean [a,*], N. Georgiou [a], R. Poirier [b], W.R. Doar III [c], D. Brill [d], D. Chauveau [a,e], C. Cerrone [a], J. Austermann [f], A. Rovere [a]

[a] University of Venice, Department of Environmental Sciences, Informatics and Statistics, Venice, Italy
[b] United States Geological Survey, Florence Bascom Geoscience Center, Reston, VA, USA
[c] South Carolina Geological Survey, Department of Natural Resources, 5 Geology Road, Columbia, SC, 29210, USA
[d] Institute of Geography, University of Cologne, Germany
[e] Geo-Ocean, University Brest, CNRS, Ifremer, UMR 6538, F- 29280, Plouzane, France
[f] Lamont-Doherty Earth Observatory, Columbia University, New York, USA

ARTICLE INFO

*Keywords:*
Interglacial
Sea-level changes
South Carolina
Luminescence dating
North America
Geomorphology
Coastal

ABSTRACT

The peak of the Last Interglacial (Marine Isotope Stage 5e; ~128–117 ky) provides a valuable analogue for understanding sea level rise under future warming scenarios. Relative sea-level (RSL) indicators from passive margins are essential for constraining past sea levels and refining glacio-hydro-isostatic adjustment (GIA) models, thereby enhancing projections of future sea-level change and associated regional impacts. In this study, we present new luminescence ages from 17 sediment samples in outcrops along the Intracoastal Waterway near Myrtle Beach, South Carolina (USA). The sampling sites lie between a series of paleo beach ridges preserved as successive off-lapping deposits, the scarp toes of which have been previously identified as indicators of the maximum sea level during each associated sea-level highstand. Our results include ages corresponding with Marine Isotope Stages (MIS) 7 (~200 ka), 5e (~125 ka), 5c (~105 ka), and the last deglacial period (~14–12 ky). These new sea-level indicators, supplemented by the existing scarp elevation data, suggest that relative sea level in this region reached similar levels during MIS 5e and MIS 5c/5a. Comparison with GIA model outputs shows that more models fit our observations (from all time periods) when a peak GMSL of less than 5 m above present during MIS 5e is assumed, which makes those scenarios more likely.

## 1. Introduction

### 1.1. Sea level and the Last Interglacial

The Last Interglacial (Marine Isotope Stage [MIS] 5e, 128–117 ky, MIS 5e hereafter) is the last period of the Earth's history when temperatures were 0.5–1.5° higher than the 1850–1900 baseline, due to different insolation forcing (Calvin et al., 2023; Dutton et al., 2015). As such, it provides an analog for future warming scenarios, albeit with the caveat that the current warming is forced by greenhouse gas emissions (Calvin et al., 2023). During MIS 5e, global mean sea level (GMSL) is traditionally reported to have peaked 5–9 m above present (Dutton et al., 2015; Dutton and Lambeck, 2012; IPCC, 2015; Kopp et al., 2009). However, recent works suggests a substantially lower MIS 5e GMSL, between 1 and 5 m above present level (Dumitru et al., 2023; Dyer et al., 2021). This could entail the possibility of asynchronous melting between Greenland and Antarctic ice sheets through MIS 5e (Barnett et al., 2023; Rohling et al., 2019), in turn causing sea-level oscillations which would manifest differently around the world due to glacial isostatic adjustment (GIA) processes (e.g. Creel and Austermann, 2024).

Coastal geological features formed during past interglacial sea-level highstands can be preserved as relic landforms or facies, and can be used as proxies to assess paleo relative sea level (RSL) and can help constrain past ice sheets and the timeline of their melting. Among these proxies, fossil beach deposits and corals (e.g. Dutton et al., 2015; Tamura, 2012) have been widely used thanks to the availability of dating techniques, such as Uranium-series disequilibrium dating of fossil corals (e.g. Cronin et al., 1981; Szabo, 1985; Wehmiller et al., 2004) and luminescence dating for beach deposits and ridges (Burdette et al., 2012; Lamothe, 2016). To understand past RSL, geological proxies (such as fossil beaches) must be transformed into sea-level index points (SLIPs). These are points with a quantifiable relationship to past sea level, a quantifiable range of uncertainty for their elevation and chronological constraints on the time of their formation or deposition (e.g. Shennan et al., 2015).

* Corresponding author.
*E-mail addresses:* silas.dean@unive.it, s.dean@studenti.unipi.it, write.me@silasdean.com (S. Dean).

https://doi.org/10.1016/j.quascirev.2025.109769
Received 17 July 2025; Received in revised form 18 December 2025; Accepted 18 December 2025
Available online 14 January 2026

The RSL obtained from any geological feature represents an estimate of local sea level (Rovere et al., 2016b) that represents the algebraic sum of GMSL and vertical land motions. Most commonly, vertical land motions can be due to the isostatic response of the crust to ice sheet growth and decay, i.e., glacial-hydro-isostatic adjustment (Mitrovica and Milne, 2003); sediment or coral reef loading and unloading, referred to as sediment or reef isostasy (Pico, 2020; Rovere et al., 2023; Simms et al., 2013); crustal tectonics (e.g. Freisleben et al., 2021); or mantle dynamic topography (Austermann et al., 2017). Disentangling these processes causing departures from GMSL and creating different RSL signals globally can be best investigated where SLIPs are particularly well-preserved, their stratigraphy is clear, and where vertical motion is either minimal or well-constrained via independent proxies or models.

In this work, we present the results of surveys of six outcrops in one such area, located along the Intracoastal Waterway (ICW). This stretch of the ICW is a ditch excavated between the 1920s and 1930s for commercial navigation, near Myrtle Beach, South Carolina, in the southeastern United States Atlantic Coastal Plain (ACP). We established new geochronologic constraints with luminescence dating, and quantified paleo RSL by assigning each facies surveyed in the field a relationship with past sea level calculated from modern wave data coupled with simple hydrodynamic equations. We compare our results to a large suite of GIA models and with uplift rates derived from older shorelines in the area, discussing the implications in terms of GMSL at the time of deposition.

### *1.2. The Pliocene-Pleistocene sea-level record from the US Middle and Southeastern Atlantic Coastal Plain*

The ACP of the United States stretches for more than 3000 km, from Florida to Cape Cod, and is often referred to as a trailing edge (or passive) margin and considered to be devoid of significant tectonic vertical land motions that would obscure the signal of sea-level changes (Doar III and Kendall 2014). However, several processes are still causing departures from GMSL, and a large corpus of chronostratigraphic work (see Fig. 1) exists to address them. The part of the coast south of Long Island, NY is beyond the former limit of the Last Glacial Maximum (LGM) Laurentide Ice sheet (LIS) (Dalton et al., 2016), so paleo-shorelines are abundant in these areas, and several authors (e.g. Doar III and Kendall, 2014) have mapped subaerial "scarps," which correspond to clastic coastal depositional environments dating back to Pliocene-Pleistocene highstands (Fig. 1, also see reviews by Muhs et al. (2003) and Rovere et al. (2015)).

From Virginia to Georgia, the presence of mollusks or corals in Pleistocene deposits (Fig. 1) allowed chronological attributions of these depositional environments thanks to different dating techniques such as amino acid racemization or U-series (see review by Wehmiller et al., 2021). In Florida, there is a transition from clastic-to carbonate-rich deposits, with extensive dating performed on the fossil coral reefs between Miami and the Florida Keys (e.g. Chutcharavan and Dutton, 2021; Hsia et al., 2024; Muhs et al., 2011; Multer et al., 2002). Several studies have also employed luminescence and electron spin resonance dating to constrain the timing of formation of beach ridge and marine deposits associated with MIS 5e and 5c (e.g. Burdette et al., 2009, 2010, 2012, 2013).

The sea-level data collected in the literature summarized above has helped identify and quantify the role of processes involved in the long-term vertical displacement of the middle and southeastern ACP. At timescales from hundreds of thousands to millions of years, mantle dynamic topography is recognized as a primary driver of vertical land motions (Hollyday et al., 2024; Moucha and Ruetenik, 2017; Rowley et al., 2013). Dynamic topography finds the clearest expression in the elevation changes of the so-called Orangeburg scarp, dated to 3 Ma (Cronin et al., 1984), which ranges in elevation from ~76 m in Virginia to ~39 m in Georgia (Rovere et al., 2015). Locally, the isostatic response to either sediment loading and unloading (Moucha and Ruetenik, 2017)

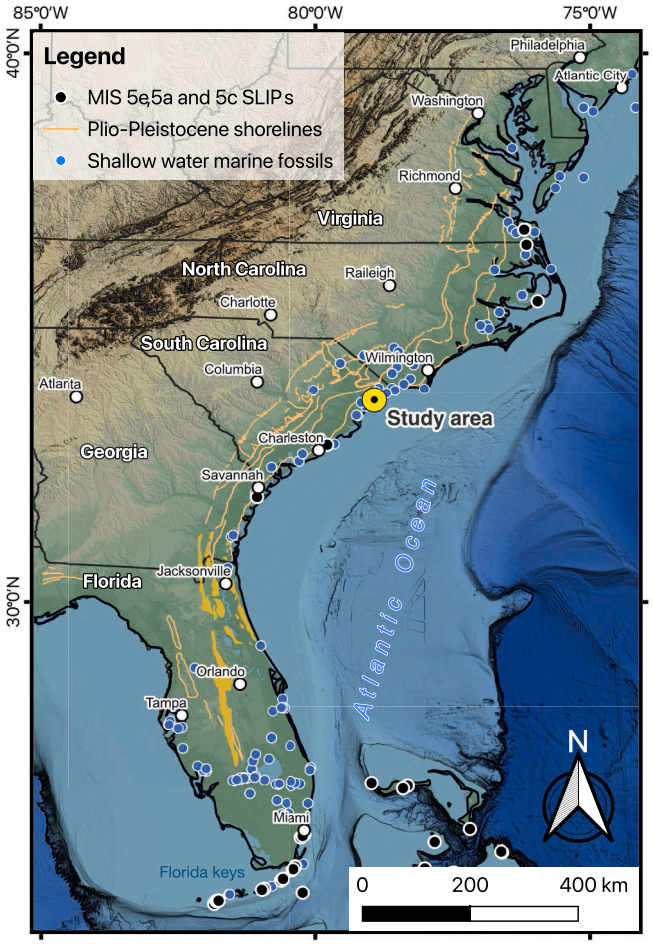


**Fig. 1.** Pliocene-Pleistocene shorelines and shallow-water marine fauna (often used as SLIPS) on the U.S. East Coast, from Virginia to Florida. Pliocene-Pleistocene shorelines were mapped by Rovere et al. (2015) from a number of sources (Ator, 2005; Dicken et al., 2005a, 2005b; Doar III, 2012; Doering, 1960; Hoyt, 1969; Schwab et al., 2009; Winker and Howard, 1977a, 1977b). Shallow-water marine fossils were extracted from the Paleobiology Database (Peters and McClennen, 2016) and the MIS 5e, 5a and 5c sea-level index points (SLIPs) were extracted from WALIS, the World Atlas of Last Interglacial Shorelines (Rovere et al., 2022). Base map from Ryan et al. (2009).

or the isostatic uplift in response to karst dissolution of Pliocene carbonates (Adams et al., 2010; Creveling et al., 2019) were considered to exert significant local departures from GMSL. GIA in response to the waxing and waning of ice sheets during the Quaternary, and in particular to the Laurentide Ice Sheet, is considered a major driver of paleo RSL changes on the ACP (Creveling et al., 2017; Engelhart et al., 2011b; Pico et al., 2017; Potter et al., 2004; Roy and Peltier, 2015). Peltier et al. (2015) estimated current GIA-induced subsidence rates (connected with post-glacial forebulge collapse) of approximately 2 mm/year in North Carolina. Later, Thompson et al. (2023) employed GIA models incorporating 3-D variation in the viscoelastic earth structure to predict the elevation of the MIS 5a highstand, which they assert peaked closer in elevation to MIS 5e GMSL than previously thought. At shorter (decadal) timescales, the CORS network station (NGS, 2024) designated SCHY and located approximately 15 km from the study area indicated 2.45 mm/year of downward vertical movement overall (Karegar et al., 2016), and Ohenhen et al. (2023) also calculated a similar rate for this study area using inSAR. Wu et al. (2022) used inSAR with data from Charleston (SC) and Wilmington (NC) to calculate total maximum subsidence (encompassing all possible processes) at 6.99 and 5.63 mm/year.

The structural geology of the area (Myrtle Beach, South Carolina) where the current study was carried out is defined by the Cape Fear Arch at the border between North and South Carolina, and the Southeast Georgia Embayment in southern South Carolina and coastal Georgia. Doar III and Kendall (2014) accept the long-term tectonic uplift rate for this area calculated by the elevation of the Pliocene Orangeburg scarp in the work of Dowsett and Cronin (1990) and Soller (1988, p. A49) of about 0.005–0.021 mm/year. Later research (Engelhart et al., 2011b) considers this estimate inadequate to capture more episodic dynamics, or explain mismatches between GIA models and Holocene sea-level datasets from the area (Engelhart and Horton, 2012). In this area, there is evidence of crustal deformation at least from the Last Interglacial to present (Marple and Talwani, 2000) with uplift rates estimated between 0.14 and 1.8 mm/year (Marple and Talwani, 2004), though it has been argued (Engelhart et al., 2011b) that such rates are not well-constrained and subject to localized effects. Van De Plassche et al. (2014) estimated tectonic uplift rates 0.23 ± 0.15 mm/year, but the precise mechanism is not certain, and the factors causing these rates have not been entirely disentangled. The uplift of the Cape Fear Arch has been attributed to a buried fault system (Marple and Talwani, 2004), but a contribution (at least in the long term, 3 Ma to present) of mantle dynamic topography is also possible (Mitrovica et al., 2020).

## 2. Materials and methods

### 2.1. Study area

The focus of this work includes six Pleistocene outcrops surveyed along the ICW near Myrtle Beach, South Carolina. In this area, a number of paleo-shorelines occur in conjunction with beach ridges (Doar III and Kendall, 2014), dating from Pliocene to the present. For the Pleistocene ridges, extensive Molluscan amniostratigraphic research exists (Wehmiller, 2013; Wehmiller et al., 1988, 2021). Doar III and Kendall (2014) summarize the history of geological research in the area and give an overview of eight offlapping geomorphic terraces or alloformations in the study area ranging in elevation from 42.6 to 3 m above sea level, dating between the Pliocene or early Pleistocene to ~34 ka. The terraces and associated alloformations are geomorphically separated by sedimentary escarpments, or "scarps". The scarps are the surficial expression of the alloformation's bounding unconformities and the scarp "toes" are the point where the later horizontal deposits meet the escarpment composed of sediment from an earlier time period (Doar III and Kendall, 2014).

The outcrops described in this study were surveyed in an area characterized by the presence of MIS 5e deposits already identified within the regional stratigraphy. The regional stratigraphic nomenclature includes different sets of names, which sometimes overlap, with each formation usually related to former RSL highstands. Our survey targets MIS 5e beach deposits from the Pamlico Formation of Doar III and Kendall (2014), or lower part of the biostratigraphically defined

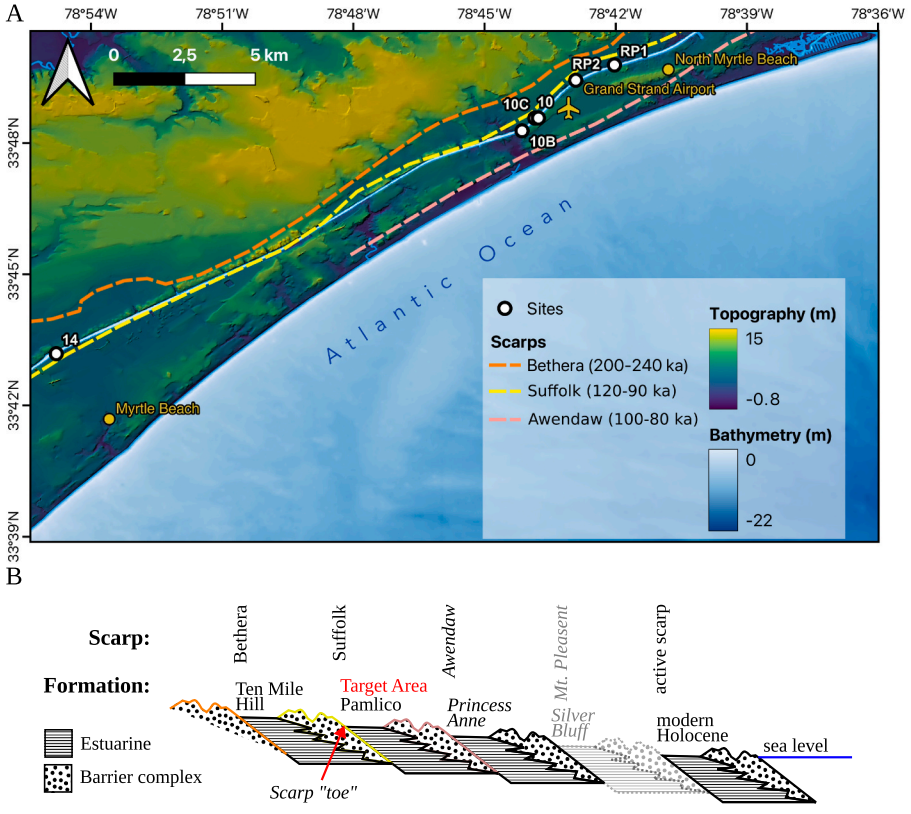


**Fig. 2.** **A**: Map of the study area, with scarps derived from Doar III (2020) and Doar (2014, 2015) and sites described in the text. Bathymetry from NOAA (NOAA, 2023) and Topography from USGS National Map (USGS, 2024). The Grand Strand Airport is referred to in much of the existing research (e.g. DuBar et al., 1980) by its former name, the Windy Hill Airstrip. **B**: Generalized profile (not to scale) illustrating the system of scarps and formations deposited by subsequent interstadials in the local area, adapted from Doar III and Kendall (2014). Colors match those of scarps in the top pane of the figure. The Mt. Pleasant and Silver Bluff Formation are faded out because though they occur in the wider region, in the immediate study area they have not been extensively mapped. This study collects samples from areas previously assessed as Pamlico to increase the chance of locating MIS 5e deposits. For detailed descriptions and locations of previously mapped facies, consult Doar III (2014, 2015).

Socastee Formation of DuBar et al. (1974). The MIS 5e deposit is also correlative to the lower part of the Wando Formation in the Charleston (SC) region to the southwest (Weems et al., 2014). MIS 5c and MIS 5a sediments (i.e., Princess Anne Formation of Doar III and Kendall, 2014), which are often found in close relation to MIS 5e material, are referred to as the upper part of the Socastee Formation of DuBar et al. (1974) or upper part of the Wando Formation by Weems et al. (2014). The underlying MIS 7 deposits are referred to as the Ten Mile Formation by Doar III and Kendall (2014) or part of the biostratigraphically defined Canepatch of DuBar et al. (1974), which however likely contains deposits from several mid-Pleistocene periods betwen MIS 7 to 11. Three of the older highstand deposits inland of the study area and their ages are identified by Doar III and Kendall (2014) as follows: Ladson Formation (MIS 11), Penholoway terrace (MIS 17 or 19), and Wicomico terrace (MIS 45–55).

The survey area selected along the ICW (See Fig. 2A for a plan view, and Fig. 2B for a generalized profile of the scarps and formations mentioned below) is ideal because in this sector the ICW is seaward of the Suffolk scarp (Doar III and Kendall, 2014), which here marks the landward extent of the Pamlico Formation (lower part of Socastee Formation or lower part of Wando, as mentioned above) deposited during MIS 5e and the start of the Ten Mile Hill Formation (or Canepatch Formation) attributed to MIS 7, which in turn has its maximum landward extent defined by the Bethera scarp. Seaward, the limit of the Pamlico is regionally marked by the Awendaw scarp (Doar III, 2020), which in turn marks the landward extent of the Princess Anne Formation, likely deposited during 5c and/or 5a; since Doar III and Kendall (2014) prefer an age of ~100-80 ka, though it is difficult to distinguish between the two phases. Mapping of 5c and 5a to the south in Charleston and Beaufort, SC (Doar, 2003; Weems et al., 2014; Willis, 2006) did discern the two highstands within a foot of each other, which could be due to base map errors or the need for more systematic RTK and luminescence data. Since they are not well differentiated here, we group the 5c and 5a together for most purposes in this study except for some discussion of GIA during 5a. In the Myrtle Beach sector, the Awendaw scarp is mapped by facies mapping with limited chronological constraints (Doar, 2014, 2015), but seaward the Mt. Pleasant scarp and the Silver Bluff Formation (the landward limit of which the scarp delineates regionally) deposited during an interstadial in MIS 3 (Doar III and Kendall 2014), is not widely mapped in the local area. In theory, deposits identified with these stages should be recognizable based on their position relative to the scarp toes (Doar III and Kendall, 2014). In reality however, the scarps in Fig. 2 are within several kilometers of each other in this area, often making difficult the association of a facies without chronological constraints to a particular stage.

The elevations of these scarp toes were also used (Doar III and Kendall, 2014) as absolute bounds for the maximum elevation of RSL highstands for each stage (though without precise age constraints) using an indicative range of ±1 m. Since this indicative range was not discussed in peer reviewed literature we use another, more conservative indicative range as discussed in the final paragraph of section 2.3 below. While in this work we use the names of these scarps, we remark that the nomenclature and identification of the corresponding deposits is not universally agreed upon, particularly since the division between different interstadials is not always fully clear. We further emphasize that the scarp elevations provide only a maximum elevation for the highstand elevation in each respective interstadial, whereas our new dates provide elevations at precise points in space and time using relationships to sea level determined by sedimentological analysis. Work on further defining chronostratigraphy was also carried out by Poirier et al. (2021) using U-series disequilibrium ages of corals, which includes a thorough re-evaluation of previously published data.

### 2.2. Survey methods

Field sites were identified using a small boat to navigate the ICW, preferring low tide for better accessibility. Suitable outcrops were cleaned of vegetation, stratigraphic logs were made, and samples taken. Bulk/dosimetry samples were taken in plastic bags from all distinct sedimentary layers, and luminescence samples were taken in facies with sufficient quartz. Samples were protected from exposure to sunlight by hammering opaque PVC tubes into the outcrop then capping first the external end and then, when extracted, the other end, after carefully filling any extra space in the tube with foam and marking the outward facing side. While the sample tubes were still in the outcrop with the label visible, a digital camera was used to capture 50–200 overlapping images per outcrop for Structure-from-Motion/MultiView Stereo (SfM-MVS) processing.

Using Agisoft Metashape, SfM-MVS processing was used to create 3-D models of the outcrops scaled to real-world distances using scalebars. Approximately 10 % of the poorest quality points (based on reprojection accuracy and reprojection error) were removed from each sparse cloud to improve quality of the final 3-D model. Medium quality depth maps with moderate depth filtering were used as a basis for final model creation to further reduce the effects of noise in the model surfaces. Orthophotos at the highest possible resolution (0.05–0.08 cm/pixel) based on the photoset were created on a viewing plane normal to the overall face of the outcrop on the XY plane but parallel to the Z axis to enable the possibility of measuring vertical elevations. Each model (with an uncertainty of 0.1 m) was benchmarked to real-world elevation with differential global navigation satellite system (GNSS) measurements that have individually calculated errors shown in Table 1.

All GNSS data were collected with a pair of EMLID REACH RS + receivers (single band) working in Real-Time-Kinematics (RTK) configuration. The position of the base station was initially set to uncorrected coordinates in the field and was corrected in post-processing using the permanent GNSS station in Longs, South Carolina (designation SCHY), maintained by the NOAA Continuously Operating Reference Station (CORS) network, located 12–30 km from our sites. GNSS data post-processing was done with Emlid Studio 1.4 (Windows version). Static processing was used in conjunction with base station data from the CORS network to refine the static receiver position, then offset the points from the rover using the base corrected position.

During the post-processing, it was noted that different elevation masks produced solutions with results that had spreads of tens of centimeters at some sites. The elevation mask blocks satellites between the specified value since satellites close to the horizon usually have noisy data (Emlid, 2025) but in some conditions may be necessary. This is likely due to the poor reception conditions in the ICW caused by factors such as the presence of water near the base station, covering of vegetation, and the walls or banks of the ICW blocking a large part of the sky. Location solutions for the static receiver at each site were processed using elevation mask values between 10 and 35°, since values above 35° rarely produced fixed solutions. The alternative solutions were assessed quantitatively and qualitatively to select the best solution based on several factors. This included clustering of different solutions, discrepancies in the X and Y dimension, and the AR ratio value of the solution, which according to the GNSS producer (Emlid, 2025) is a measure of quality of the solution. All elevation data were referred to NAVD88 from the GNSS ellipsoid height using the online VDATUM tool by the US National Oceanic and Atmospheric Administration (https://vdatum.noaa.gov/vdatumweb/).

### 2.3. Indicative meaning

To transform any geological sea-level proxy into a sea-level index point (SLIP) (Khan et al., 2019), i.e., a feature with a quantifiable relationship to a paleo sea level, it is necessary to quantify its relationship with sea level at the time of formation (Shennan, 1986; Shennan et al., 2015). This relationship, called the indicative meaning, is usually obtained by quantifying the reach above or below sea level of modern coastal processes or the living ranges of fossil organisms found *in situ* (e.

**Table 1**
Luminescence ages obtained in this study. Name CLL and Lab. Code are designations used by the Luminescence dating facility. Facies refers to the facies identified in the main text. Mineral refers to the type of material used in the analysis. N = number of aliquots. Age errors are 1σ. Sample elevations are relative to NAVD88 datum, while elevation errors derive from GNSS measurements as described in the main text.

| Lab. code | Site | Facies | Site Lat. | Site Lon. | Mineral | N | Over-dispersion (%) | Burial dose (Gy) | Dose rate (Gy/ka) | Age (ka) | Age error (ka) | Sample elevation (m NAVD88) | Sample elevation error (m) |
|---|---|---|---|---|---|---|---|---|---|---|---|---|---|
| C-L5484 | 10B | SEMS | 33.8047 | −78.7357 | Quartz | 30 | 21 ± 3 | 64.7 ± 2.6 | 0.45 ± 0.02 | 143.0 | 8.5 | 1.30 | 0.11 |
| C-L5485 | 10B | SEMS | 33.8047 | −78.7357 | Quartz | 28 | 22 ± 3 | 54.8 ± 2.4 | 0.45 ± 0.02 | 121.8 | 7.5 | 1.50 | 0.11 |
| C-L5486 | 10B | SEMS | 33.8047 | −78.7357 | Quartz | 18 | 22 ± 4 | 53.7 ± 3.0 | 0.45 ± 0.02 | 119.1 | 8.4 | 1.64 | 0.11 |
| C-L5487 | 10B | LD | 33.8047 | −78.7357 | Quartz | 16 | 25 ± 5 | 56.1 ± 3.7 | 0.55 ± 0.02 | 102.7 | 8.2 | 3.93 | 0.11 |
| C-L5488 | 10B | LD | 33.8047 | −78.7357 | Quartz | 19 | 17 ± 3 | 58.7 ± 2.5 | 0.59 ± 0.03 | 100.0 | 6.1 | 4.12 | 0.11 |
| C-L5489 | 10B | LD | 33.8047 | −78.7357 | Quartz | 21 | 14 ± 3 | 59.1 ± 2.0 | 0.63 ± 0.03 | 94.1 | 5.3 | 4.27 | 0.11 |
| C-L5490 | 10B | UD | 33.8047 | −78.7357 | Quartz | 20 | 37 ± 6 | 11.7 ± 1.6 | 0.78 ± 0.03 | 14.9 | 2.1 | 5.05 | 0.11 |
| C-L5491 | 10B | UD | 33.8047 | −78.7357 | Quartz | 21 | 31 ± 5 | 11.0 ± 0.8 | 0.79 ± 0.03 | 14.1 | 1.2 | 5.20 | 0.11 |
| C-L5492 | 10B | UD | 33.8047 | −78.7357 | Quartz | 21 | 28 ± 5 | 10.1 ± 0.8 | 0.8 ± 0.04 | 12.6 | 0.9 | 5.10 | 0.11 |
| C-L5493 | 10B | SHCB | 33.8047 | −78.7357 | Quartz | 17 | 13 ± 3 | 57.0 ± 2.1 | 0.46 ± 0.02 | 124.4 | 7.6 | 3.01 | 0.11 |
| C-L5494[a] | 10B | CBBD | 33.8047 | −78.7357 | Quartz | 39 | 29 ± 3 | 47.4 ± 2.4 | 0.49 ± 0.09 | 96.8* | 6.8 | 3.43 | 0.11 |
| C-L5494 | 10B | CBBD | 33.8047 | −78.7357 | Feldspar | 23 | 17 ± 3 | 115.9 ± 4.1 | 0.96 ± 0.11 | 120.9 | 15.0 | 3.43 | 0.11 |
| C-L5495[a] | 10B | CBBD | 33.8047 | −78.7357 | Quartz | 39 | 17 ± 2 | 45.9 ± 1.4 | 0.48 ± 0.02 | 95.4* | 5.5 | 3.47 | 0.11 |
| C-L5495 | 10B | CBBD | 33.8047 | −78.7357 | Feldspar | 23 | 21 ± 3 | 130.6 ± 5.8 | 0.95 ± 0.11 | 137.4 | 17.6 | 3.47 | 0.11 |
| C-L5482 | 10 | CBBD | −33.8095 | 78.7295 | Feldspar | 23 | 19 ± 3 | 129.8 ± 5.7 | 1.01 ± 0.11 | 128.0 | 7.0 | 2.30 | 0.06 |
| C-L5498 | 10C | SEMS | 33.8095 | −78.7308 | Quartz | 12 | 25 ± 6 | ≥85 | 1.43 ± 0.05 | ≥60 | | 1.99 | 0.07 |
| C-L5498 | 10C | SEMS | 33.8095 | −78.7308 | Feldspar | 14 | 10 ± 2 | 210.7 ± 6.2 | 1.91 ± 0.12 | 110.0 | 8.0 | 1.99 | 0.07 |
| C-L5505 | RP2 | LD | 33.8238 | −78.7152 | Quartz | 14 | 26 ± 5 | 42.3 ± 2.7 | 0.3 ± 0.02 | 143.0 | 12.0 | 2.78 | 0.35 |
| C-L5504 | RP2 | PIGD | 33.8238 | −78.7152 | Feldspar | 23 | 18 ± 3 | 259.0 ± 10.8 | 1.27 ± 0.11 | 204.0 | 19.0 | 2.34 | 0.35 |
| C-L5508 | RP2 | PIGD | 33.8238 | −78.7152 | Quartz | 11 | 33 ± 8 | ≥117 | 0.65 ± 0.02 | ≥180 | | 1.97 | 0.35 |

[a] indicates ages rejected as outlined in the main text.

g. Hibbert et al., 2016). This is often achieved using a modern analog (e.g. Horton and Edwards, 2005; Rovere et al., 2016b). The elevational range of occurrence of a sea-level proxy is called "indicative range", while the offset between the modern analog and a specific tidal datum (often mean sea level) is referred to as "reference water level" (Shennan et al., 2015). Each SLIP must then be assigned an age with a quantifiable uncertainty range.

A SLIP by itself represents only the elevation of RSL at a certain point in time and space. Some features do not indicate a precise relationship to sea level, but only show the maximum or minimum possible sea level. As an example, a beach-dune contact identified within the stratigraphic context (e.g. Cann and Murray-Wallace, 2012) will indicate that sea level was below the contact. Aeolian sand dunes, as subaerial landforms, provide a maximum possible sea level, since the sea level at the time must have been below the elevation at which they formed. The features that only show a maximum possible paleo sea level are called "terrestrial limiting points", while features that show only the minimum possible sea level are referred to as "marine limiting points" (Rovere et al., 2016b).

Due to intense human development of the Myrtle Beach area, using the modern coast to identify relationships between coastal facies and sea level might be misleading. For this reason, we here established the indicative meaning using the approach proposed by Rovere et al. (2025) and Lorscheid and Rovere (2019), which entail the calculation of wave runup elevations and breaking depths to assess, respectively, the upper and lower limits of the indicative range. To do this, we extracted tide data from the FES2022 tidal model (Carrere et al., 2022) at a point slightly offshore Myrtle Beach. The model outputs match well with the high-low water levels measured daily at the Springmaid Pier (NOAA, 2025) tide gauge at Myrtle Beach (NOAA ID 8661070, Fig. S1). Then, we extracted wave data for a point offshore Myrtle Beach from the Copernicus Marine Environment Monitoring Service (CMEMS) WAVeReanalYSis (WAVERYS) (Law-Chune et al., 2021). Both wave and tide data were extracted for a total of about 43 years, from Jan 1st, 1980 to September 30th, 2023. Both wave height and period (respectively, Figure S2 And Figure S3) match well with those measured at the NOAA buoy. To calculate the runup values using the above approach (Rovere et al., 2025) we used beach slope values from 2506 points measured along the Cape Fear Arch from Doran et al. (2024).

For beach shore facies or deposits that can also be deposited below sea level, we calculated the breaking depth (**db**) of waves using the formula adopted by Lorscheid and Rovere (2019) from Lee and Mizutani (2010):

$$\frac{db}{L_0} = \left(3.86\beta^2 - 1.98\beta + 0.88\right)\left(\frac{H_s}{L_0}\right)^{0.84}$$

Where $\mathbf{H_s}$ is the significant wave height of incident waves (extracted from the WAVERYS data mentioned above), $\beta$ is the average beach slope from the data mentioned above ($\beta = 0.04$), and $\mathbf{L_0}$ is the wavelength, that is derived from the period as follows:

$$L_0 = \frac{gT_p}{2\pi}$$

Where $\mathbf{g}$ is the gravity constant (9.81 m/s$^2$) and $\mathbf{T_p}$ is the mean deep-water wave period.

A similar approach to the one outlined above can be adopted for the scarp toes that were mapped in this area (Doar III and Kendall, 2014), which mark the highest RSL during a highstand. These features were assigned the same indicative meaning as the inner margin of marine terraces following the quantification of the upper and lower limits proposed by Rovere et al. (2016a) (storm wave swash height to breaking depth). The calculated results for these values are shown in section 3.2.1 below.

### 2.4. Luminescence dating

Luminescence dating was conducted at the Cologne Luminescence Laboratory using coarse-grain quartz (100–200 μm) for 17 sediment samples. For three of these plus two additional samples, coarse-grain (150–180 μm) potassium feldspar extracts were analysed. Sample tubes were opened under dimmed red-light conditions. Sample preparation included dry sieving, treatment with HCl (10 %) to remove carbonates, with $H_2O_2$ (10 %) to remove organic matter and with sodium oxalate (10 %) to destroy clay aggregates. Density separation with sodium polytungstate was used to extract potassium-rich feldspar (<2.58 g/cm$^3$) and quartz (>2.62 g/cm$^3$ and <2.68 g/cm$^3$). Quartz samples received a final etch with HF (40 %) for 40 min to remove any feldspar contamination and the alpha-radiation-affected outer rim of the grains. A 60 min HCl rinse was performed after HF etching.

Dose rates are based on radionuclide contents of the samples derived with high-resolution gamma spectrometry with an Ortec PROFILE M-Series GEM Coaxial P-type gamma spectrometer and the conversion factors of Guérin et al. (2011). Water contents were determined by measuring water loss after heating the samples at 50 °C until completely dry. For two of the samples (C-L5494 and C-L5495), dose rates of stratigraphically heterogeneous sections (i.e., facies variations within the range of gamma radiation around the samples) were reconstructed using the layer model of Riedesel et al. (2022). Internal dose rates for feldspar extracts are based on empirical potassium contents of 10 ± 2 % (Smedley et al., 2012). The alpha radiation contribution in feldspar is calculated with an a-value of 0.11 ± 0.02 (Kreutzer et al., 2014). Cosmic dose rates were estimated based on geographic location, depth below surface and a sediment density of 1.8 ± 0.1 g/cm$^3$ following Prescott and Hutton (1994). Calculation of total dose rates was based on the online calculator DRAC (Durcan et al., 2015). Data related to dose rate calculation are summarized in Spreadsheet S2 for all samples.

For burial dose determination, quartz and feldspar extracts were fixed on steel discs using silicone spray to create aliquots with 2 mm (quartz) or 1 mm (feldspar) diameter. All discs were measured on Risø TL/OSL DA-20 readers equipped with $^{90}Sr/^{90}Y$ beta irradiation sources delivering ~0.1–0.2 Gy/s at the sample position. Luminescence signals were stimulated with blue LEDs (~470 nm) at 125 °C (quartz) and infrared LEDs (~870 nm) at 50 and 290 °C (feldspar), and detected through 7.5 mm Hoya U340 (quartz) or 410 nm interference filters (feldspar). All quartz measurements followed a standard SAR protocol (Murray and Wintle, 2000) with preheat at 180 °C for 10 s and a cutheat at 160 °C. Feldspar samples were measured with a post-infrared-infrared protocol at an elevated temperature of 290 °C (pIRIR$_{290}$, Thiel et al. (2011). Dose rates are recorded in Spreadsheet S2 and measurement protocols are summarized in Spreadsheet S3.

The appropriateness of the quartz protocol was tested with a preheat-plateau test for a selected sample by increasing the preheat temperature in steps of 20 °C from 180 °C to 280 °C. The cutheat was always 20 °C below the associated preheat temperature. The test indicates equivalent doses independent of preheat temperatures between 180 °C and 240 °C. In addition to that, dose-recovery tests at 180 °C demonstrate adequate reproducibility of laboratory doses in the range of the natural dose for all quartz samples (dose recovery ratios of 3 aliquots per sample deviate by less than 10 % from unity for all samples, i.e. laboratory doses between ~10 Gy and ~90 Gy). The pIRIR protocol was evaluated using dose-recovery tests and residual dose measurements (3 aliquots per sample) after signal resetting in a Dr. Hönle Sol2 solar simulator for 24 h. Dose-recovery ratios range between 0.98 and 1.01, laboratory residual doses remain below 8 Gy for all samples.

Equivalent doses were measured for 11–39 aliquots (quartz) or 14–23 aliquots (pIRIR290) per sample. Due to comparably low equivalent dose scatter for all samples (over-dispersion below 30 % after removing outliers with equivalent doses more than 2-sigma above or below the mean) and ~normally distributed dose values (Fig. S11), burial doses were calculated using the central age model (CAM; Galbraith et al. (1999) for all samples. Signal saturation (i.e., more than 30 % of saturated aliquots; defined as saturated when their natural signal was larger than the 2xD0 criterium of a single saturation exponential function) was observed for quartz samples C-L5498 and C-L5508, resulting in minimum quartz ages. Due to low sample-dependent g-values of 0.4–1.8 %/decade for the pIRIR$_{290}$ signal determined following the approach of Auclair et al. (2003), pIRIR290 ages were not corrected for signal loss due to fading. Data related to burial dose determination are summarized in Table 1 for all samples.

### 2.5. Granulometry

Granulometric analysis was performed using a Malvern Mastersizer 3000 Laser Diffraction machine with Hydro EV attachment to prevent settling of coarse materials in the reservoir. The sediments were centrifuged twice with deionized water to remove salts. HCl treatment to remove carbonate fraction (a significant percent of mass for many samples) consisted of treatment in a fume hood with open containers in beakers of water with 8–10 % hydrochloric acid which was refreshed until all reaction ceased. Sediments were again centrifuged twice with distilled water to remove any leftover acid. The samples were then placed in a fume hood in open beakers on a hotplate at 50 °C with 7–8 % $H_20_2$ and deionized water to remove the organic fraction, which was refreshed daily until all reaction ceased. Before and after each stage of treatment, the samples were dried in an oven at 50 °C then weighed to obtain the fractions by mass of salts, carbonates, and organics. Prior to insertion in the Mastersizer 3000, the sediments were then placed in jars with 0.2 % hexametaphosphate on shakers overnight, then immediately placed in the Mastersizer with 180 s of sonication to break up aggregations. Grain size results are reported in the supplementary material as Spreadsheet S1. Further details of this spreadsheet are in the readme of the supplementary materials. Most of the grain-size laboratory work was carried out by Laura Alessandrini with guidance from S. Dean and A. Rovere as part of a B.Sc internship and thesis (Alessandrini, 2024).

### 2.6. Glacial isostatic adjustment

To evaluate our RSL observations in light of GIA processes, we use the set of 576 GIA model scenarios previously published by Barnett et al. (2023) with timesteps of 0.5 ky during the LIG. The parameter space encompassed by the GIA models consists of standard and accelerated Termination II (MIS 6) deglacial timing, a lithosphere thickness of 71 or 96 km, a lower mantle viscosity from 3 to 40 × 10$^{21}$ Pa s, a range of upper mantle viscosity from 0.3 to 0.5 × 10$^{21}$ Pa s, and six models that also correspond to different thicknesses of the Laurentide Ice Sheet (LIS) and thus different distributions of global ice at the penultimate glacial maximum. The six ice models, ordered from largest LIS to the smallest, are as follows: ICE-6G, L6G-32, L6G, L6G-47, Colleoni, and Lambeck (for information about the individual models consult Barnett et al., 2023 and references therein). The solutions set GMSL to zero during the LIG in order to isolate GMSL from observations (Dyer et al., 2021).

As the GIA models employed assume a GMSL of 0 m for the duration of MIS 5e (Dyer et al., 2021), we assessed ranges for MIS 5e GMSL from three different published studies: Dumitru et al. (2023) with a range of 1.0–2.7 m; Dyer et al. (2021) with a range of 1.2–5.3 m; and the IPCC AR5 (2015) of 5.0–10.0 m. This was done by adding the three GMSL ranges separately in turn to the RSL value of the model outputs during the LIG (~128-117 ky) to the entire duration of the LIG. As the GIA solutions span tens of meters, we created a subset of predictions by selecting only those solutions where MIS 7, MIS 5e, and MIS 5c/5a highstand RSL matches the elevation of, respectively, the Bethera, Suffolk and Awendaw scarp toes as mapped by (Doar III and Kendall, 2014) within their indicative meaning and matching the timing of the highstands by the ice and GIA models. For the MIS 5e, the range of indicative range of the scarp has to overlap the range of the RSL provided by the GIA model and GMSL range.

## 3. Results

We surveyed six outcrops (see Fig. 2 for location) along the ICW and produced luminescence ages from four of them (Table 1) for a total of 17 dated samples. Two of the quartz ages (C-L5498, C-L5508) provide only a constraint on the latest possible deposition of the sediments, while two quartz ages (from C-L5494 and C-L5495) were ruled out for reasons discussed in the SHCB subsection of the results below. For these two samples, as well as C-L5498, the pIRIR290 signal was assumed to provide more accurate ages. As concerns the assignation of dates to specific highstands, it is important to highlight that it is highly improbable that the vast majority of our chronological data (except from the ages that we

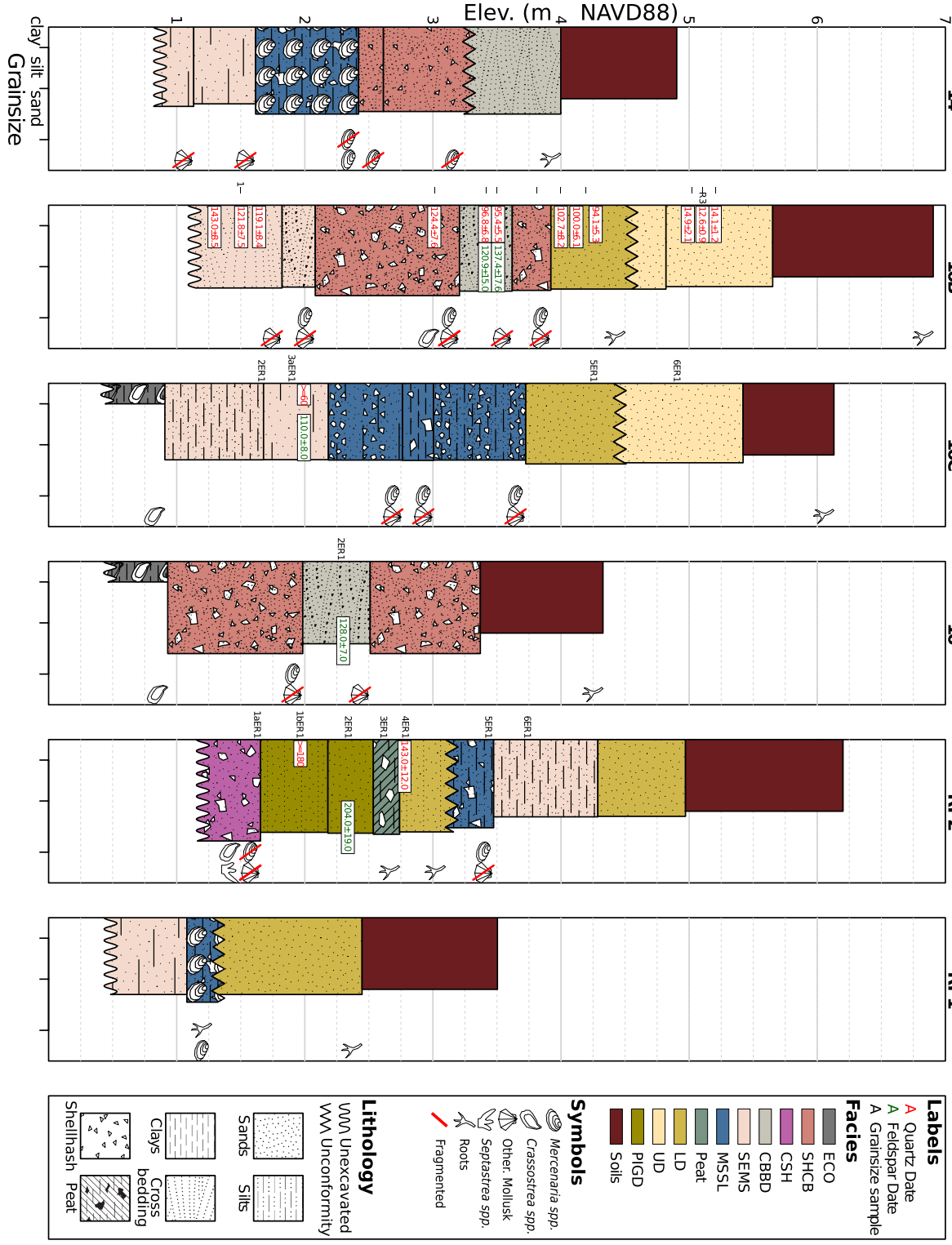


**Fig. 3.** Stratigraphic columns for the six sites surveyed in the study area. Facies acronyms are defined in the text. Elevation is relative to the local NAVD88 datum. This datum 0 is at 0.136 mean sea level (MSL) according to the local NOAA tide gauge at Springmaid Pier, Myrtle Beach SC (NOAA, 2025). Grain size for outcrops 14 and RP1 are based on field assessment. Diagrams created with StratigrapheR (Wouters and Smith, 2022).

correlate with MIS 7) statistically correspond with marine highstands older than MIS 5. Even if we look at 3-sigma uncertainty intervals (99.7 % probability), there is no overlap with MIS 7 (or older) for all samples that we correlate with MIS 5.

We identified ten different facies related to different coastal environments forming at different times during the Pleistocene. Their main sedimentological, geological and paleo environmental characteristics are described below and shown in Figs. 3 and 4. Grain Size is referenced according to the Wentworth scale (Wentworth, 1922). Detailed grain size results are available in the supplementary materials Spreadsheet S1. The facies are described below generally from oldest to youngest. The interpretation of each facies in terms of sea level is contained in section 3.2 of the discussion below.

### 3.1. Identified facies

**Consolidated shell hash (CSH).** This facies is a highly consolidated shell hash found at RP2 within a bimodal matrix consisting predominantly of coarse to very coarse reddish-brown sand, with a minor fraction of fine to very fine sand. Shell fragments also included a specimen of highly abraded *Septastrae spp.* coral, and mollusks (such as *Mercenaria* clams and, and *Crassostrea* oysters and some small (<2 cm) intact *Mulinia* clam shells. The carbonate fraction in this facies can reach up to 32 % by mass. These characteristics indicate deposition in a high-energy nearshore environment. No luminescence ages were obtained from this deposit, but its position beneath aeolian sands dated to 204 ± 19 ka (C-L5504) at site RP2 suggests correlation an interstadial either MIS 7 or an earlier stage such as MIS 9 or MIS 11. This interpretation is supported by the depositional sequence of scarps outlined in Doar III and Kendall (2014), and the close proximity of older scarps in the area. The *Septastrea spp.* coral found could also be reworked from an older deposit due to its highly abraded condition.

**Estuarine clay with oysters (ECO).** This sediment, present at the limit of the exposed base of sites 10 and 10C, is composed primarily of dark gray clay containing abundant *Crassostrea virginica* (Eastern oyster) shells. The lithology and fossil content suggest an estuarine setting with limited wave energy. Although undated in the current study, its stratigraphic position—relative to other dated facies—implies either a possible MIS 7 age or earlier (if intervening sediments were removed by erosion) or an early MIS 5e age, formed under transgressive estuarine conditions where coarse sediments were not transported.

**Peat**. A black, organic-rich peat layer was identified only at site RP2, within medium to coarse sands. It contains modern root intrusions/root casts, ~6 % organic matter by mass, and ~6 % carbonate. The peat represents a marshy, low-energy environment. Thickness ranges from about 0.1 to 0.3 m. At RP2, this layer underlies sands dated to 143 ± 12 ka (C-L5505), and overlies a PIGD deposit with ages of 204 ± 19 ka (pIRIR290; C-L5504 2-R1) and >180 ka (quartz; C-L5508 1 b-R1), indicating it formed prior to MIS 5e. This layer could either represent the base of the transgressive sequence leading to the MIS 5e highstand, or the top of a regressive sequence following after an earlier highstand, most likely corresponding with MIS 7.

**Pre-interglacial dune (PIGD).** Identified only at site RP2, this facies comprises aeolian sands from an interstadial in MIS 7 or possibly MIS 6 due to the wide age uncertainty of the only dated sample. It consists of medium to coarse unimodal sand arranged in alternating reddish-brown and yellowish-brown bands, likely the product of post-depositional processes (e.g., oxidation, soil formation). The unimodal grain-size distribution, lack of substantial fine fractions or carbonate and the banded coloration are characteristic of aeolian deposition. The sands however have a coarser mode (~1 phi) than post-MIS 5e dunes in the area, which exhibit modes closer to 2 phi. pIRIR290 dating at RP2 yielded an age of 204 ± 19 ka (C-L5504). A quartz age from the sediments in RP2 yielded an age constraint of≥180 ka (C-L5508).

**Silty estuarine and marine sands (SEMS)**. This facies, found at 14, 10B, 10C, RP2, and RP1, includes cross-bedded medium sand and silty fine sand, reflecting variable energy conditions. The cross-bedded beige or tan sand is typically unimodal, medium-grained, and contains ~10 % carbonate (mostly <1 mm shell fragments), suggesting deposition in a relatively calm marine setting. The silty sands are bimodal, with a dominant coarse/medium sand mode and a secondary silt/clay mode (~10 % by volume), again with a similar carbonate fraction. These features indicate a lower-energy estuarine or shallow marine environment. SEMS often overlies or underlies higher-energy beach deposits. It occurs roughly coincident with MIS 5e and, based on luminescence ages, was dated to both pre-MIS 5e times (e.g., 143.0 ± 9 ka at site 10B; C-L5484), during MIS 5e (at site 10B from 121.8 ± 7.5 ka [C-L5485] and 119.1 ± 6.4 ka [C-L5486]) and the period immediately following MIS 5e (110 ± 8 ka at site 10C; C-L5498). The earlier age from ~143 ka at 10B must be viewed with skepticism in the context of two additional ages only a few centimeters above with ages from ~121.8 to ~119.1 ka. This facies can be viewed as corresponding to estuarine or transgressive conditions in MIS 5e.

**Shell hash with cross-bedding (SHCB)**. This facies, identified at sites 14, 10B, and 10, consists of unconsolidated shell hash within a reddish-brown or tan, coarse sand matrix. The carbonate fraction is 40–50 % by mass and includes broken or abraded shells of various sizes—some entire *Mercenaria* spp. shells, oyster fragments (*Crassostrea virginica*), and other biogenic remains. Cross bedding is visible in certain sites in parts of the deposits though less apparent in other parts. Often interbedded with cross-bedded beach deposits, the SHCB signifies a high-energy coastal environment. At site 10B, it was dated to MIS 5e (124 ± 8 ka; C-L5493). At site 10, this shell hash brackets cross-bedded beach deposits (CBBD, see below) that were dated to 128 ± 7 ka (C-L5482).

**Cross-bedded beach deposits (CBBD).** Interbedded with, or adjacent to, the SHCB, these deposits identified at 14, 10B, and 10 consist of cross-bedded, unimodal medium to fine tan or yellowish-brown sand with ~25 % carbonate (mostly small shell fragments <2 cm). pIRIR290 luminescence dating in two sites indicates MIS 5e deposition: Site 10B - 137 ± 18 ka (C-L5495) and 121 ± 15 ka (C-L5494), and Site 10 – 128 ± 7 ka (C-L5482). The ages from 10B for this facies were dated first with quartz and yielded ages of 95 ± 6 ka (C-L5495) and 97 ± 7 ka (C-L5494). These are assumed to be inaccurate since no visible unconformity exists between this deposit and the underlying SHCB in the same outcrop, and a higher MIS 5c RSL relative to MIS 5e is also not demonstrated by the local stratigraphy (Doar III and Kendall, 2014). The problematic quartz ages are possibly related to incorrect quartz dose rates, since these are the only samples with apparently heterogeneous gamma radiation fields. Our pIRIR290 ages are less sensitive to external dose rate errors due to nearly 50 % of the dose rate in the low radiation environment of the beach ridges coming from internal potassium contents. The pIRIR290 ages collectively tie the CBBD facies to beach conditions during MIS 5e.

***Mercenaria* shell bed/Storm layer (MSSL).** A polymodal deposit found at sites 14, 10C, RP2, and RP1 characterized by large concentrations of mollusk shells within a mixed sand-silt matrix of greyish or beige color. At some sites (e.g., Site 14), *Mercenaria* spp. shells dominate—a few are articulated in life position, but most are fragmented or disturbed. Elsewhere, razor clams, small periwinkle-like gastropods (~1 cm, typical of marshy or brackish environments), and/or chaotic shell accumulations appear in discrete horizons, suggesting multiple depositional or lag events. The poorly sorted matrix (coarse and fine fractions) and the abundance of shell debris imply episodic, high-energy storm activity that reworked estuarine or subtidal deposits into beach sands. This facies typically lies above or below the SEMS. Ages from sites 10C and RP2 underlie it at 110 ± 8 ka (C-L5498) and 143 ± 12 ka (C-L5484), implying that these events occurred during MIS 5.

**Lower dune (LD).** These generally unimodal sands, found at sites 10B, 10C, RP2, and RP1, are of gray or beige color overlie shell hash, silty sand, or storm deposits and peat (at RP2). They have modes in the medium to coarse sand range, with negligible carbonate or organic

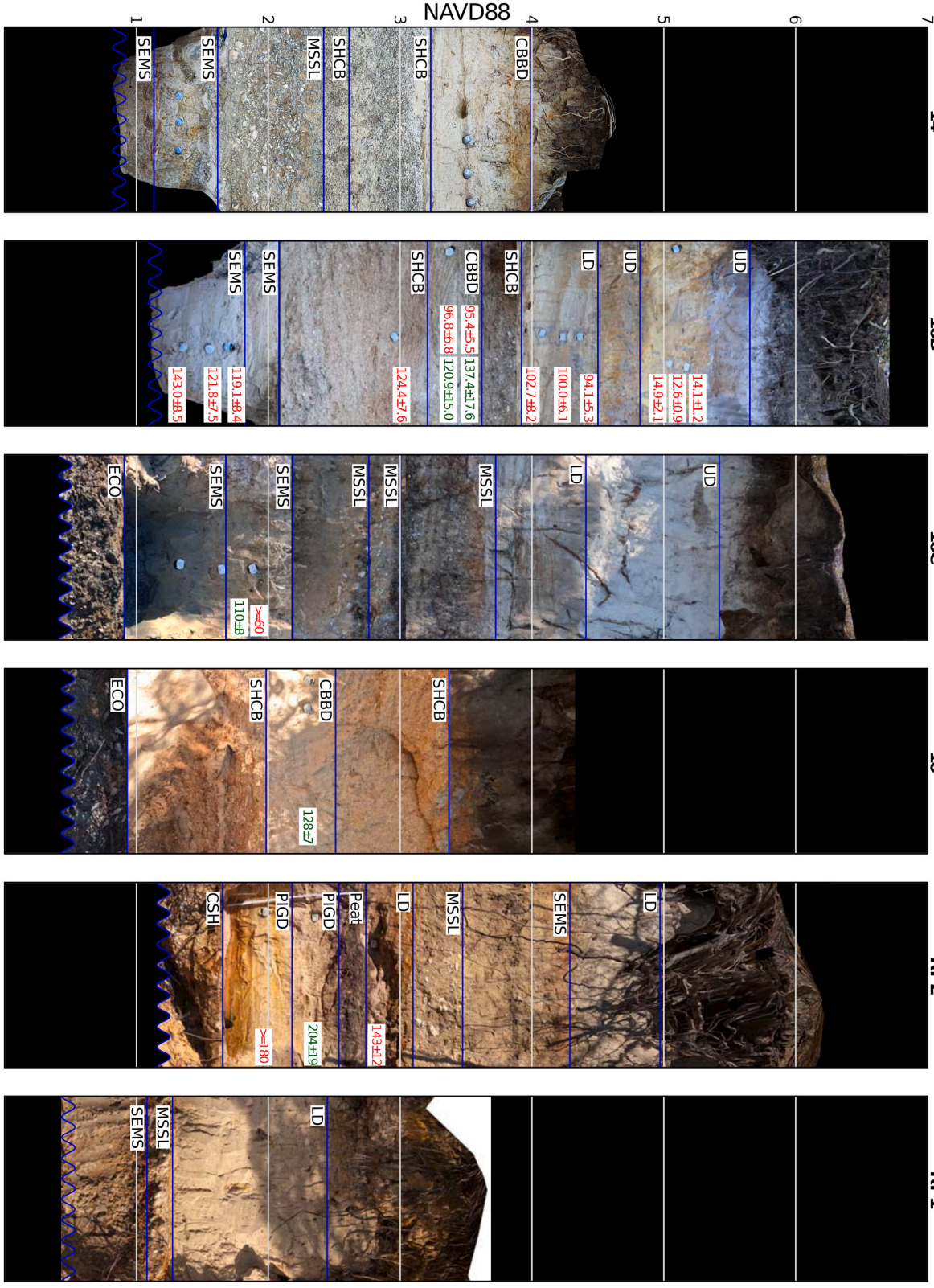


**Fig. 4.** Compilation of representative orthophotography (derived from photogrammetry) and photographic material derived from the current study's survey showing different facies from each of the outcrops discussed in this paper. Note: The orthophotography has been altered to simply present a to-scale vertical succession of all the sediments in the outcrop. For the full orthophotos, see the supplements. Red numbers are quartz luminescence ages, green numbers are feldspar luminescence ages. The black letters are facies (see Table 2 and section 3.1 of the results).

content. Because they often occur near the present surface, modern or submodern roots and vegetation are commonly observed. Colors vary from beige to grayish. At site 10B, the LD sands facies was dated to MIS 5c and unconformably overlies the MIS 5e shell-hash, with ages of 103 ± 8 ka (C-L5487), 100 ± 6 ka (C-L5488), and 94 ± 5 ka (C-L5489).

**Upper Dune (UD).** Overlying unconformably (based on dating from 10B) the LD, this facies, found at 10B and 10C is sedimentologically similar to the LD—mainly medium to coarse, unimodal beige, tan or yellowish-brown sand—but differs in color, likely due to leaching and soil formation. At site 10B, it yielded post–LGM, deglacial luminescence ages: 15 ± 2 ka (C-L5490), 13 ± 1 ka, (C-L5492), and 14 ± 1 ka (C-L5491).

### 3.2. Sea-level interpretation

#### 3.2.1. Sea-level index points

Among the facies we identified, SHCB and CBBD are related to former sea level by the presence of cross-bedding, which is commonly associated with the upper shoreface (Tamura, 2012) The coarse grain size of these two facies (medium to coarse sands), is, along with the heavily worn and fragmented marine shell matter present, also indicative of an high-energy shore environment. Since the modern analogues for these facies may be observed along a vertical range in the literature (Tamura, 2012 and ref. therein) and in a variety of settings (for example in the swash zone, bars, and troughs with varying degrees of protection from wave energy), we do not differentiate these two facies in the indicative range quantification. The consolidated shell hash (CSH) facies from outcrop RP2 could also be used in a similar way, but we did not obtain any ages from it, precluding its use as SLIP.

We assume that these facies can form anywhere from the upper reach of waves (swash zone, corresponding to the maximum runup) to the breaking depth. To conservatively estimate the normal limits of the swash zone, we use wave runup calculated from wave models following the approach of Rovere et al. (2025) (Fig. 5) and verified against wave and tidal data from Myrtle beach as reported in the methods section. We calculate that, in this area, the 50th percentile of runup is 1.1 m above sea level. We use the 50th percentile of the runup not only because locally this facies' modern analog is informally observed up to merely the lower swash zone, but also because in literature (e.g. Tamura, 2012) this kind of crossbedding is not associated with the subaerial foreshore or extreme waves. Facies formed by extreme waves (MSSL) identified elsewhere in our survey have a more polymodal grain-size distribution and more heterogenous preservation of mollusks. On the other side of the indicative range, for the breaking depth, we use the significant wave height extracted from the wave models (1.5 m) and the average peak wave period (7.8s). Using the formulas reported in the methods sections, we calculate that the breaking depth at our study site is −1.70 m. We use the upper (1.1 m) and lower (−1.7 m) bounds of the indicative meaning to calculate the reference water level and indicative range of the SHCB and CBBD facies as shown in Rovere et al. (2016a) (Table 2, Fig. 6).

The scarps identified in Doar III and Kendall (2014) can be considered SLIPs marking the peak of the highstand, and using as storm wave swash height the 99th percentile of runup values shown in Fig. 5 (2.5 m) and the breaking depth calculated above for the Myrtle Beach area (−1.7 m), we calculate that the reference water level associated with any scarp in this area is 0.4 m and the indicative range is 4.2 m.

#### 3.2.2. Limiting points

Several of the other facies identified in our work (Table 2) can be interpreted as marine or terrestrial limiting points. The peat is not linked to sea level because it lies between aeolian deposits that cannot be precisely linked to RSL and peat formation is often associated stratigraphically with transgressive conditions (e.g. Flint et al., 1995) such as those found leading up to the MIS 5e highstand, or with regressive strand plains and gradual sea-level drops. These peats have been noted throughout the area in past studies (DuBar et al., 1980; Hollin and Hearty, 1990), for example at the site designated as WA56 near the Grand Strand Airport (formerly known as the Windy Hill Airstrip). The SEMS and ECO facies are here interpreted as marine-limiting points, indicating the minimum paleo sea level because these facies must be deposited in underwater environments but at a more variable depth below sea-level (although not deep marine) that does not significantly constrain sea level.

In contrast, the UD, LD, and PIGD aeolian deposits are considered terrestrial limiting points that define the maximum possible sea level, because as discussed in Tamura (2012), the precise elevation or relationship relative to sea level depends on a variety of temporally and spatially specific factors at the beach face. The MSSL facies is not used as

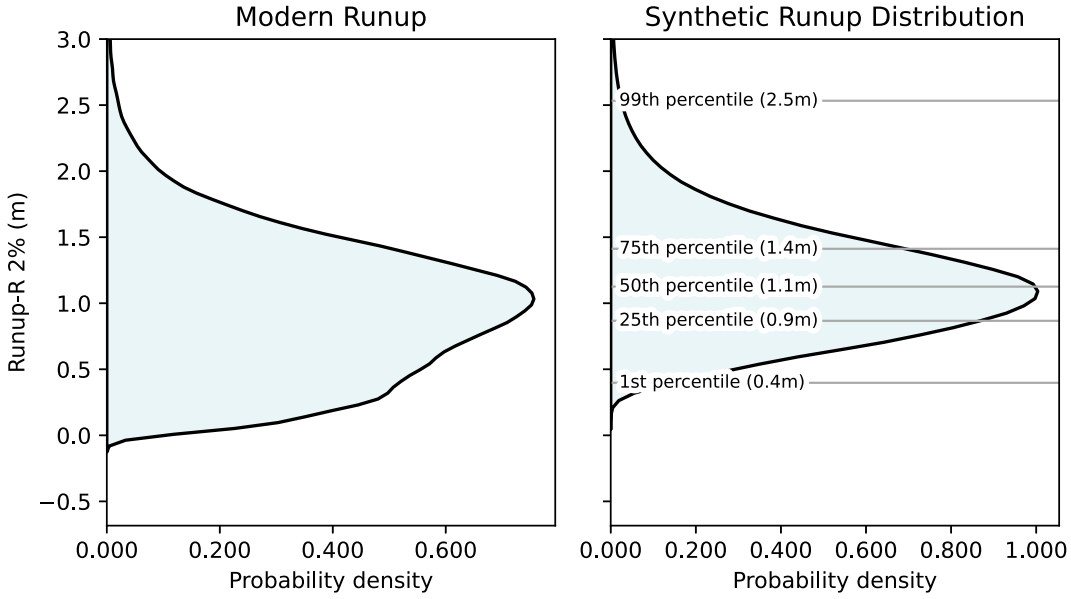


**Fig. 5.** Left: Probability density plots representing simulated 2 % wave runup (R2) at Myrtle Beach between 1980 and 2024, for waves with directions perpendicular to the coast and reaching the coast in tidal conditions from MSL to high tide. Right: Probability density plot representing simulated 2 % wave runup at Myrtle Beach for a synthetic dataset including all potential combinations of tide stages and waves measured historically. The gray lines show the 1, 25th, 50th, 75th and 99th percentiles of this distribution.

**Table 2**
Marine limiting (ML), terrestrial limiting (TL) and sea-level index points (SLIP) in the Myrtle Beach area, with ages and highstand assignment. The scarps are derived from Doar and Kendall (2014), with the indicative meaning calculated as reported in the text.

| Sample | Outcrop | Facies | Indicator Type | Reference water level (m) | Indicative range (m) | RSL (m) with 1-sigma uncertainty (elevation for ML and TL) | Age (ka) with 1-sigma uncertainty | Stage attribution |
|---|---|---|---|---|---|---|---|---|
| C-L5484 | 10B | SEMS | ML | | | 1.3 ± 0.15 | 143 ± 8.5 | Pre MIS 5e |
| C-L5485 | 10B | SEMS | ML | | | 1.5 ± 0.15 | 121.8 ± 7.5 | MIS 5e |
| C-L5486 | 10B | SEMS | ML | | | 1.6 ± 0.15 | 119.1 ± 8.4 | MIS 5e |
| C-L5487 | 10B | LD | TL | | | 3.9 ± 0.15 | 102.7 ± 8.2 | MIS 5c |
| C-L5488 | 10B | LD | TL | | | 4.1 ± 0.15 | 100 ± 6.1 | MIS 5c |
| C-L5489 | 10B | LD | TL | | | 4.3 ± 0.15 | 94.1 ± 5.3 | MIS 5c |
| C-L5490 | 10B | UD | TL | | | 5.1 ± 0.15 | 14.9 ± 2.1 | Deglacial |
| C-L5491 | 10B | UD | TL | | | 5.2 ± 0.15 | 14.1 ± 1.2 | Deglacial |
| C-L5492 | 10B | UD | TL | | | 5.1 ± 0.15 | 12.6 ± 0.9 | Deglacial |
| C-L5493 | 10B | SHCB | SLIP | −0.3 | 2.8 | 3.3 ± 1.41 | 124.4 ± 7.6 | MIS 5e |
| C-L5494 | 10B | CBBD | SLIP | −0.3 | 2.8 | 3.7 ± 1.41 | 120.9 ± 15 | MIS 5e |
| C-L5495 | 10B | CBBD | SLIP | −0.3 | 2.8 | 3.8 ± 1.41 | 137.4 ± 17.6 | MIS 5e |
| C-L5482 | 10 | CBBD | SLIP | −0.3 | 2.8 | 2.5 ± 1.43 | 128 ± 7 | MIS 5e |
| C-L5498 | 10C | SEMS | ML | | | 2.0 ± 0.12 | 110 ± 8 | MIS 5e |
| C-L5505 | RP2 | LD | TL | | | 2.8 ± 0.36 | 143 ± 12 | Pre MIS 5e |
| C-L5504 | RP2 | PIGD | TL | | | 2.3 ± 0.36 | 204 ± 19 | MIS 7 |
| Bethera scarp toe | | | SLIP | 0.4 | 4.2 | 10.3 ± 2.1 | | MIS 7 |
| Suffolk scarp toe | | | SLIP | 0.4 | 4.2 | 6.3 ± 2.1 | | MIS 5e |
| Awendaw scarp toe | | | SLIP | 0.4 | 4.2 | 4.8 ± 2.1 | | MIS 5a/5c |

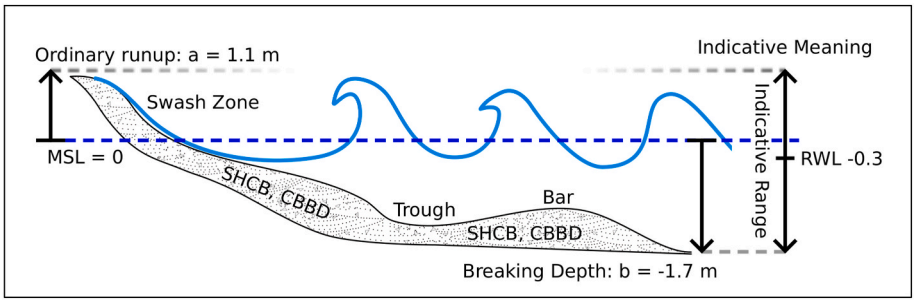


**Fig. 6.** Graphical representation of the indicative meaning for the sea-level index points in this study. The indicative meaning consists of the indicative range (a span of 2.8 m) and the reference water level (−0.3 m).

a limiting point of either kind, as this could be either thrown up onto the shore beyond the normal reach of the waves during extreme events, or washed into estuarine settings below sea level.

## 4. Discussion

We compare our new luminescence ages and paleo sea-level interpretations with previously mapped Pleistocene scarp-toe highstands (Doar III and Kendall, 2014). Since the study area is located close to the former margins of the Laurentide Ice Sheet (LIS), we also compare these data to GIA model predictions in a parameter space of varying ice and earth parameters.

Comparing the GIA model solutions to the local scarp-toe elevations (used as RSL index points deposited during the highstands of MIS 7, MIS 5e, and MIS 5a/5c), the highest number of models matching GIA predictions is obtained either with the GMSL range of Dumitru et al. (2023) (GMSL 1.0–2.7 m above present, 45 models out of 576) or that of Dyer et al. (2021) (GMSL 1.2–5.3 m above present, 51 models out of 576). Only 13 out of 576 model solutions match the higher MIS 5e GMSL range used by the IPCC (2015) (GMSL 5–10 m above present). If we assume ten hypothetical GMSL range scenarios for the 5e from 0 to 10 m each with a 1 m range, we note that the scenarios between 0 and 3 m each have ~40–50 models matching, above which the amount of matching models drops off rather linearly until 5 m after which matches are much fewer until 9 m, beyond which no models match.

The matching GIA solutions tend to be those that had standard deglacial timing during Termination II following MIS 6 (see Supplemental Fig. S4), along with mid-to-high upper mantle viscosity and mid-to-high lower mantle viscosity. Ice models with larger Laurentide Ice sheet volumes also have a greater tendency to match the local scarp toe RSL. The Colleoni model used in Barnett et al. (2023) had no MIS 7 RSL highstands above MIS 5e, so no solutions using that ice model match. In the Bahamas as discussed in Dyer et al. (2021), it was instead the lower Laurentide Ice Sheet volumes that better matched the data, and the slower Termination II rates. This contradiction does indicate the limitations of this method, but the inability to match our data with many of the GIA models with the high 5–10 m range for MIS 5e GMSL does support the likelihood of the lower GMSL ranges for MIS 5e. We note that the models we considered only varied in 1-D Earth structure, not GMSL history, (except for the speed of termination II between ~160-128 ka) and assume an MIS 7c and 7a GMSL highstand of 0 m and −10.5 m, respectively, and highstands for 5c and 5a of approximately −21 and −19 m.

### 4.1. MIS 7 and earlier

Peak MIS 7 GMSL is usually reported as being lower than present-day (−5 to −15 m, (Siddall et al., 2007), though the GIA model dataset we use includes a peak of 0 (see Fig. 7). In terms of RSL, higher than present values have been reported elsewhere as a result of GIA (Rowe et al., 2014), and in the immediate study area the scarp toe of the Ten Mile Hill (or Canepatch Formation) dated to MIS 7 abuts the Bethera scarp (Doar and Kendall, 2014; Rowe et al., 2014) with a calculated RSL of 10.3 ± 2.1 m. GIA causes local RSL to be consistently above GMSL at this location during most of MIS 7 (Barnett et al., 2023; Dyer et al., 2021). The GIA models used in this study that match the elevations of the

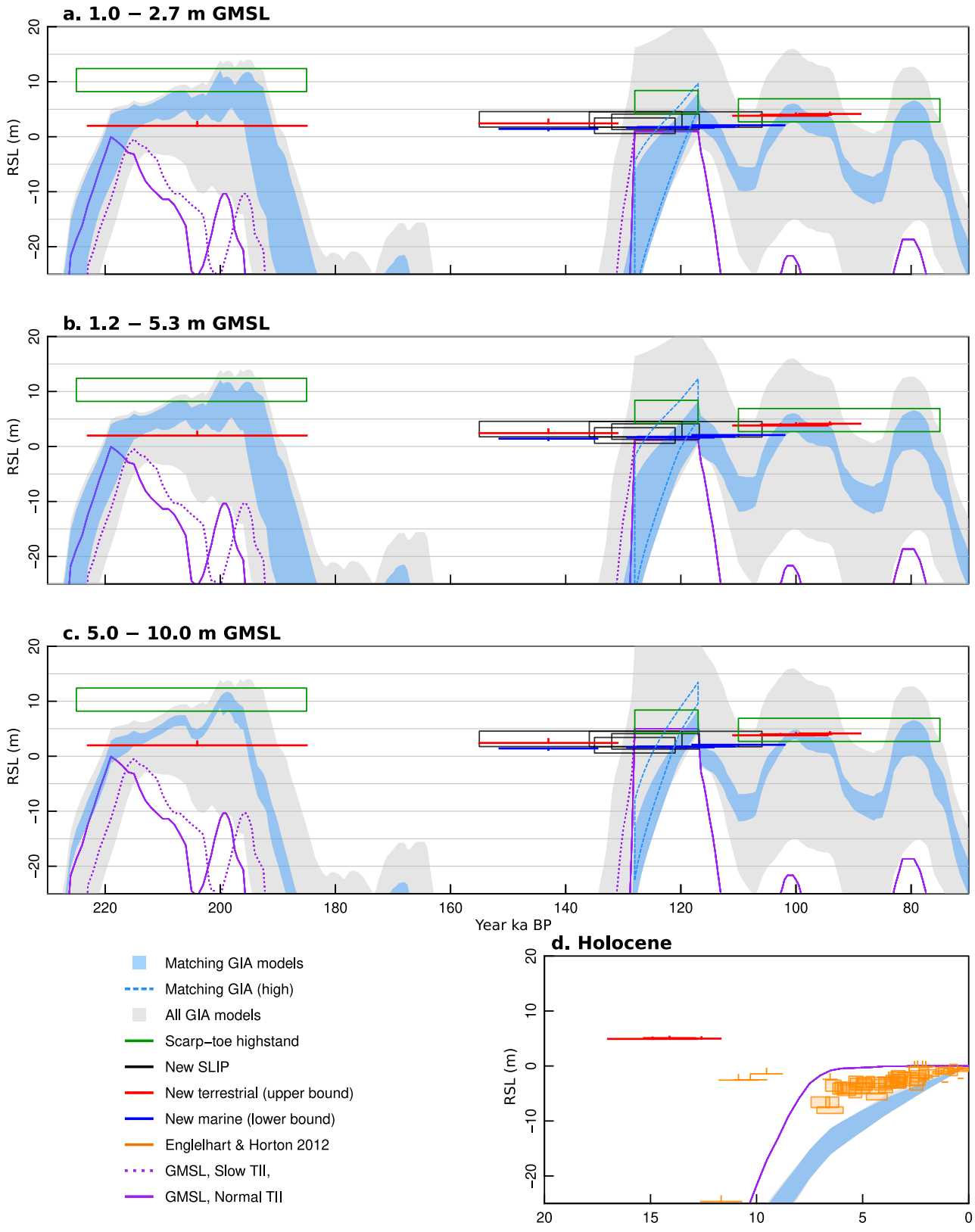


**Fig. 7.** Comparison between modelled and observed RSL at Myrtle Beach, South Carolina. Panels a, b, c represent GMSL scenarios for the MIS 5e from Dumitru et al. (2023), Dyer et al. (2021) and the IPCC-AR5, respectively. The GIA models shown in gray are the entire set of 576 solutions described in Barnett et al. (2023) using the GMSL history of Waelbroeck et al. (2002), with the lower range of each MIS 5e GMSL scenario added. The blue polygon is all the models, with each MIS 5e GMSL scenario added, which match the three scarp elevations during the highstands, also plotted with the lower part of the MIS 5e GMSL range. The dotted blue line represents the higher part of the range of each MIS 5e GMSL scenario. Panel d. shows the Deglacial dunes dated in this study and the Holocene dataset from Engelhart and Horton (2012) using the GMSL range of Dumitru et al. (2023).

scarp-toe highstands (in all three MIS 5e GMSL scenarios), are all solutions in which the highest highstand of the stage is MIS 7a rather than MIS 7c (which take place at ~220-215 ka and ~200-195 ka respectively in these ice models), though the model parameter space does include solutions with a higher highstand in 7c.

The oldest deposits we surveyed were the consolidated shell hash (CSH) that underlie aeolian dunes dated to 204 ± 19 ka (PIGD, C-L5504). This age has a large chronological uncertainty that makes it difficult to assign it to a particular interstadial. It seems likely that the dunes were deposited during the drop in sea level after MIS 7a. The CSH below this sample represents a higher-energy nearshore or estuarine coastal environment with a significant carbonate fraction from mollusk fragments at an elevation up to 1.6 m NAVD88 (or ~1.5 m above MSL) (See Fig. 3) and could be associated with an older interstadial from *at least* MIS 7, if not older. Just as much of the MIS 7 deposits in this area would end up being eroded, recycled, or redeposited during the subsequent MIS 5e highstand, the sediments in the CSH themselves could contain many reworked materials from an older stage than that of ultimate deposition, making identification challenging; likewise, relic deposits would also sometimes be reoccupied (Doar III and Kendall, 2014 and ref. therein). The area surveyed in this paper lies near the scarp toe of both the Suffolk and Bethera scarps, so the MIS 11-7 beach deposits are all likely to closely underlie MIS 5 material in the way described in Doar III and Kendall (2014, Fig. 3 therein) with a likelihood of erosional unconformities.

### 4.2. MIS 5e

Our new data confirms that RSL was higher than present at some point between ~130-110 ka within the limits of precision imposed by the RSL reconstructions and luminescence dating uncertainties (Fig. 7a–c). Uncertainties of several thousand years on our luminescence ages do not allow for precise considerations on the timing of RSL or elevation of the peak highstands during this interglacial, but RSL as measured by the new sea-level points is between 2.5 and 3.8 m ± 1.4 m. The dated samples in 10B (Fig. 3) are not from the highest extent of the shell hash with cross bedding (SHCB) facies visible in the outcrop, which is about half a meter higher. Additionally, there appears to be an erosional unconformity between these facies and the 5c aeolian deposits above (LD). Such a scenario agrees with the mapping done by Doar III and Kendall (2014), who use the elevation of the Suffolk Scarp (with a calculated RSL of 6.3 ± 2.1 m above present sea level) as the highest MIS 5e RSL.

These data tend to support the idea that GMSL during this highstand would not surpass 5 m above present, because we found that few GIA model solutions match local RSL conditions at this site if we assume a MIS 5e GMSL between 5 and 10 m. This agrees also with other recent works which constrain MIS 5e GMSL between 1 and 5 m above present (Barnett et al., 2023; Dumitru et al., 2023; Dyer et al., 2021). Our new luminescence-dated SLIPs from this stage tend to be slightly earlier (see Fig. 7a and b) than the modelled RSL peak when assuming a relatively flat GMSL curve, e.g. of Dumitru et al. (2023) during MIS 5e. Were these SLIPS used to constrain the GIA model subset along with the scarps, it still would match more models with lower GMSLs ranges such as the Dumitru et al. (2023), but many would be eliminated from the subset in all three scenarios because modelled sea-level rise at this site above 0 m in MIS 5e occurs slightly later than indicated by these luminescence ages. Many of the possible models (usually with normal Termination II rates rather than the slower models) that have an RSL nearing 0–5 m in the beginning of the LIG usually have highstands above the indicative range of the MIS 5e Suffolk scarp toe's calculated RSL. This disparity between the luminescence and the GIA model could indicate earlier highstands or fluctuations that are not reflected in the models. In this stage we also have four marine limiting points, imposing lower bounds for sea level. In all three GMSL scenarios, two of these from outcrop 10B (C-L5486 and C-L5485) fit well with the MIS 5e highstand, while one (C-L5498 from outcrop 10C) is young enough to be from either MIS 5c or MIS 5e given the dating uncertainty. A final marine limiting point from 10B (C-L5484) appears to be too old regardless of the GMSL scenario. As suggested in the results section, this could be a dating issue, since the two other 10B marine limiting points lie only 20–30 cm above this sample. If however, we consider the 2 sigma range of the age instead of the 1 sigma, it could also support an earlier highstands or fluctuation not represented in the model subsets. There is also a terrestrial limiting point from aeolian sediments from site RP2 (C-L5505) at 143.0 ± 12.0 ka elevation 2.8 m NAVD88. Considering the younger limit of the 1 sigma age this also can fit into all three GMSL scenarios.

More context for the MIS 5e RSL in the wider region comes from Szabo (1985), who obtained an open system U-Th MIS 5e age in corals from the Mark Clark Pit (McCartan et al., 1982) in Charleston (South Carolina), approximately 170 km SW down the coast from our study area. These corals were collected from near MSL, in the unit identified as the Pamlico Formation (Doar and Kendall, 2014), or lower part of the Wando Formation (Weems et al., 2014), which (as mentioned above) extends up to 6.8 m above MSL, and provides a calculated RSL of 6.3 ± 2.1 m above present for sea level using our indicative meaning calculation. A lower bound comes in the form of an open-system coral age (Szabo, 1985) from the Windy Hill Airport site (Grand Strand airport) that most likely corresponds to MIS 5e, and was collected (McCartan et al., 1982) at approximately 4 m above MSL from the Socastee Formation (Pamlico). Szabo (1985) reports the age appears too young, but it appears plausible with our data. If this point is taken as a minimum elevation it also appears to be in agreement with the results of our work. In regard to closed-system U-series in South Carolina, only 9 dates are known (Wehmiller et al., 2004). These are attributed not to 5e, but to the subsequent stage 5a. The authors of the current study are not aware of any published closed-system U-series ages from MIS 5e north of the Florida Keys. This highlights the importance of the current study in establishing, through the new luminescence dating, the presence of 5e deposits in the Lower Socastee Formation. The new 5e ages, along with those from the other stages discussed below, also represent useful additional chronological constraints to supplement the extensive existing aminostratigraphy in the area (e.g. Wehmiller et al., 2004; Wehmiller et al., 2021).

### 4.3. MIS 5c and 5a

Following MIS 5e, sea level fell and rose again twice before MIS 4. The models we use (Barnett et al., 2023; Dyer et al., 2021) assume GMSL peaks for 5c and 5a of approximately −21 and −19 m. The peak GMSL during these two highstands (MIS 5c, ~100 ka, and MIS 5a, ~80 ka) however has been the source of debate, with some literature (e.g. Lambeck and Chappell, 2001) proposing they peaked 20–30 m below present level, and corals from these stages appearing at approximately −20 m below present in Barbados (Bard et al., 1990). Later work by Tawil-Morsink et al. (2022) estimates GMSL during 5a between −10 and −33 m below present (95 % confidence) based on the Barbados corals. Research which incorporates data from the SE ACP (Thompson et al., 2023; Thompson and Creveling, 2021 and refs therein) has suggested that later MIS 5 interstadials were characterized by GMSL peaks at −9.4 ± 5.3 m for 5c (Creveling et al., 2017), and −13 m (Thompson et al., 2023) or −8.5 ± 4.6 m (Creveling et al., 2017) during 5a. Recent work from reef cores in Florida (Hsia et al., 2024) has suggested that 5a RSL there was more than 2 m higher than formerly estimated, which might also indicate the necessity of changes to the GMSL curve for this stage. Another avenue of research — investigations of phreatic growths on speleothems in Mallorca (Dorale et al., 2010) has even indicated that 5a GMSL could have peaked as high as +1 m above present due to past overestimation of the GIA contribution in that region.

The 5c and 5a RSL highstands are found at similar elevations in the current study area, with 5c not always distinctly above 5a in the greater region (Doar and Kendall, 2014). Doar III and Kendall (2014) use for the

Princess Anne Formation an age range of ~100-80 ka from swash zone corals (Wehmiller et al., 2004) at a highstand RSL of 4.8 ± 2.1 m based on the Awendaw scarp toe elevation. As indicated in the previous section, the 9 dates from Berkely Pit, Rifle Range Pit, and Jones Pit in Wehmilller et al. (2004) used to assess the age of the Princess Anne Formation constitute the only closed-system U-series ages in the state of South Carolina. As concerns the GIA model set, none of the model solutions matching this area's scarp elevations in any of our three GMSL scenario have significantly disparate highstand elevations for 5c and 5a (see Fig. 7a–c): Rather, those matching solutions that have either the 5c or 5a highstand within the scarp's elevation range have both at similar levels. Likewise, the matching models, in all three GMSL scenarios, are mixed between having a higher peak in 5a and a higher peak in 5c, but the elevation difference between these two interstadials is always less than 5 m, as in the local mapping.

Though no SLIPS from MIS 5c were identified, one sea-level minimum indicated by silt marine and estuarine sands (SEMS, C-L5498 from outcrop 10C) was dated to near the end of MIS 5e (~110 ka) and MIS 5c beach dunes unconformably overlay MIS 5e SLIP facies at site 10B with three ages C-L5487, C-L5488, C-L5489). These aeolian dune limiting points from ~110-90 ka do fit the subset of selected GIA models in all three MIS 5e GMSL scenarios (Fig. 7a–c), because subsetting of models in the MIS 5e depends more on Termination II timing, and less on earth model parameters, so the subsets matching to MIS 7 and MIS 5c/5a are not dramatically different under different 5e GMSL scenarios. The existing research and new data in this study area support a local RSL in MIS 5c and 5a at elevations not far below MIS 5e.

In an attempt to test whether some of the higher estimates of GMSL (Creveling et al., 2017; Thompson et al., 2023) during these interstadials could fit our data, we set both MIS 5c and 5a GMSL to −9 m. In the GIA outputs used in this study, this requires adding ~13 m and 10 m to the MIS 5c and 5a GIA solutions. There were no matching models for these requirements, because they do not reconcile with the relatively low RSL attested by the scarp's elevation in this stage, and, for 5c, by the elevation of our new aeolian terrestrial limiting points at approximately 4 m. In the broader SE ACP instead, Thompson et al. (2023) and Pico et al. (2017) list indicators of RSL in North Carolina from Parham et al. (2013) of MIS 5c and 5a which are sometimes several meters higher than the MIS 5e elevations we find in Myrtle Beach. Laminated sands in Edward Pit (North Carolina) dated to MIS 5c sit at 10 m, and in Pamlico county (North Carolina) sands from MIS 5c sit at 7.4 m, and to the east of that site, a sand deposit from MIS 5a overlies MIS 5c at the Suffolk shoreline with a calculated relative sea level of 11.5 m (Parham et al., 2013; Pico et al., 2017; Thompson and Creveling, 2021) though Pico et al. (2017) considers the latter as terrestrial limiting points. MIS 5a RSL is usually reported above present sea level by other works in North and South Carolina. This is the case for samples from Moyock North Carolina (attributed variously to both 5c and 5a in the cited references), where deposits containing corals were dated with U-series analysis, as well as coral deposits in Charleston, South Carolina, and beach deposits dated by luminescence and U-series in Pamlico Sound, North Carolina (Cronin et al., 1981; Szabo, 1985; Thompson and Creveling, 2021; Wehmiller et al., 2004). Had we found higher elevations from these interstadials, such as those collated from existing studies by Pico et al. (2017), it would likely be easier to conclude higher MIS 5c or 5a GMSL, but we do not have any dated material from MIS 5a, and our current material when compared to the GIA models does not support such findings. Whether this can be ascribed merely to inadequately constrained Pleistocene-term vertical motion in the Cape Fear Arch (see below) or to features of the GIA models we use, is not possible for us to say.

### 4.4. Post MIS 5 to Holocene

After MIS 5a, GMSL fell well below present in MIS 4, MIS 3 and MIS 2, though the middle ACP does contain RSL evidence from e.g. MIS 3 near to and above sea level within 10 m (Pico et al., 2017) from terrestrial and marine limiting points. These consist of sands and ridges from Virginia and North Carolina (Mallinson et al., 2008; Parham et al., 2013; Scott et al., 2010). Our samples however, present a lacuna for most of this time period since the main focus of the survey was the Last Interglacial. At ~14-12 ka however, a dune was deposited in Myrtle Beach as sea level started to rise towards its present-day position. We obtained luminescence ages (C-L5490, C-L5491, C-L5492) for this dune because it unconformably overlies the 5c dune sands below it at outcrop 10B, with nothing to indicate the time gap between the two aeolian deposits. This is far above the GIA predictions (see Fig. 7d) which in this time period converge within several meters of elevation.

Starting at ~7 ka, a sea-level record on the US East Coast was imprinted in a series of saltmarshes that provide a high-resolution reconstruction of the second half of the Holocene (Engelhart and Horton, 2012). A significant phenomena in the US southeastern Atlantic Coast, as well as in the middle Atlantic and some of northeast Atlantic, is that this Holocene saltmarsh RSL dataset (Engelhart and Horton, 2012) and other regional RSL reconstructions like Ramsey et al.'s (2022) reconstruction from the middle Atlantic Delmarva coastal/estuarine organic deposits are consistently above GIA predictions by several meters (Fig. 7d), just as the deglacial dune samples dated in this study appear to be. Engelhart et al. (2011a) rule out sediment compaction and tidal changes as the source of this discrepancy. Long-term deformation (which might be caused by mantle convection or sediment loading) can be calculated using the elevation of the middle Pliocene Orangeburg scarp.Doar III and Kendall (2014) use this approach to accept rates of 0.005–0.021 mm/year (Cronin et al., 1984; Soller, 1988), which are too small to explain this discrepancy in the Holocene data - model comparison.

Using the differences in rates reconstructed from RSL histories at a variety of sites along the East Coast, Van De Plassche (2014) estimated an uplift of 0.24 ± 0.15 mm/year on the Cape Fear Arch of an episodic/oscillatory nature on longer geologic time scales but of uncertain cause. If this was indeed a long-term tectonic uplift rate operating only in one direction, it would have caused 20–30 m of uplift since MIS 5e and more since MIS 7, which would be at odds with the present-day elevation of our RSL data and the previously mapped scarps. Alternatively, as a way to reduce the gap between data and observations during the Holocene, Kuchar et al. (2019) explore GIA models with lateral variations in viscosity and find that those can improve the fit, providing a possible explanation for the observed misfit. From our GIA dataset, that the models with higher mantle viscosity values tended to match better the earlier highstands in this area might indicate the need for the model parameter space to incorporate higher viscosity values. This also highlights the need to include lateral variability in Earth structure in GIA runs that extend over the late Pleistocene (Austermann et al., 2021; Thompson et al., 2023).

## 5. Conclusions

This study presents new luminescence ages of 17 samples from MIS 7 to just before MIS 1 from the Intracoastal Water Way, Myrtle Beach sector. These ages provide four sea-level index points from MIS 5e ranging from 2.5 to 3.8 m ± 1.4 m above present MSL, using wave models to determine indicative meanings via a method that is globally applicable to beach facies. We also provide 12 marine and terrestrial limiting points that can be used to delimit the maximum and minimum paleo relative sea level during MIS 7, MIS 5c, and Deglacial. These reconstructions agree well with suggested highstand elevations previously mapped in the study area using scarp-toe elevations. These luminescence ages can also supplement an existing corpus of extensive local chronostratigraphic ages. This study supports a local relative sea level (including the effects of glacio-hydro-isostatic adjustments) of approximately 3–7 m in the Myrtle Beach area during the Last Interglacial, and also supports the possibility of MIS 5e global mean sea level being below 5 m. These conclusions are particularly important if MIS 5e is considered

an analog for future sea level rise caused by anthropogenic climate change.

## Credit statement

Dean, S.: Conceptualization, Methodology, Software, Validation, Formal Analysis, Investigation, Data curation, Writing - original draft, Writing - review & editing, Visualization, Supervision, Project administration Georgiou, N.: Software, Formal Analysis, Investigation, Writing - review & editing Poirier, R.: Conceptualization, Methodology, Validation, Investigation, Writing - review & editing, Supervision, Project administration, Funding acquisition Doar, W.R. III: Conceptualization, Methodology, Validation, Investigation, Writing - review & editing, Supervision, Project administration Brill, D.: Formal Analysis, Investigation, Resources, Writing - review & editing Chauveau, D.: Validation, Formal Analysis, Writing - review & editing Cerrone, C.: Validation, Formal Analysis, Writing - review & editing Austermann, J.: Conceptualization, Methodology, Software, Validation, Formal Analysis, Resources, Data curation, Writing - review & editing, Visualization, Supervision, Funding acquisition Rovere, A.: Conceptualization, Methodology, Software, Validation, Formal Analysis, Investigation, Resources, Data curation, Writing - original draft, Writing - review & editing, Visualization, Supervision, Project administration, Funding acquisition.

## Declaration of competing interest

The authors declare that they have no known competing financial interests or personal relationships that could have appeared to influence the work reported in this paper.

## Acknowledgments

This paper is a result of the WARMCOASTS project, funded by the European Research Council (ERC) under the European Union's Horizon 2020 research and innovation programme (grant agreement n. 802414). This paper reflects views of the authors and the EU is not responsible for any use that may be made of the information it contains. JA acknowledges support from NSF grant EAR 24-20482 and RP received partial funding for this work from the United States Geological Survey Land Change Science Program in the Ecosystems Mission Area. Any use of trade, firm, or product names is for descriptive purposes only and does not imply endorsement by the U.S. Government. Laura Alessandrini contributed assistance with the investigation and data curation of grain-size analysis data. Flavia Visin and Alessandro Bonetto provided technical assistance for grain-size analysis. John Wehmiller corresponded with the authors and provided access to datasets of study sites. Michael Toomey and Thomas Cronin reviewed the manuscript internally at USGS. The co-authors from Ca'Foscari would like to thank P.J. Hearty for hosting us for discussion and refreshment after the survey.

## Appendix A. Supplementary data

Supplementary data to this article can be found online at https://doi.org/10.1016/j.quascirev.2025.109769.

## Data availability

All data and/or code is contained within the submission. The supplementary material will also be made available in the Zenodo repository linked to Digital Object Identifier 10.5281/zenodo.17848247 available through the URL https://doi.org/10.5281/zenodo.17848247.

## References

Adams, P.N., Opdyke, N.D., Jaeger, J.M., 2010. Isostatic uplift driven by karstification and sea-level oscillation: modeling landscape evolution in north Florida. Geology 38, 531–534. https://doi.org/10.1130/G30592.1.

Alessandrini, L., 2024. Analisi Granulometrica Tramite Diverse Tecniche Analitiche Di Campioni Di Sedimenti Costieri Prelevati Lungo La Costa Est Degli Stati Uniti (South Carolina) Datati All'Ultimo Interglaciale (125 Ka) (B.Sc Thesis). University of Venice Ca'Foscari, Venice, Italy.

Ator, S.W., 2005. A Surficial Hydrogeologic Framework for the Mid-atlantic Coastal Plain. US Department of the Interior, US Geological Survey.

Auclair, M., Lamothe, M., Huot, S., 2003. Measurement of anomalous fading for feldspar IRSL using SAR. Radiation measurements. Proceedings of the 10th international Conference on Luminescence and Electron-Spin Resonance Dating (LED 2002) 37, 487–492. https://doi.org/10.1016/S1350-4487(03)00018-0.

Austermann, J., Hoggard, M.J., Latychev, K., Richards, F.D., Mitrovica, J.X., 2021. The effect of lateral variations in Earth structure on Last Interglacial sea level. Geophys. J. Int. 227, 1938–1960. https://doi.org/10.1093/gji/ggab289.

Austermann, J., Mitrovica, J.X., Huybers, P., Rovere, A., 2017. Detection of a dynamic topography signal in last interglacial sea-level records. Sci. Adv. 3, e1700457. https://doi.org/10.1126/sciadv.1700457.

Bard, E., Hamelin, B., Fairbanks, R.G., 1990. U-Th ages obtained by mass spectrometry in corals from Barbados: sea level during the past 130,000 years. Nature 346, 456–458. https://doi.org/10.1038/346456a0.

Barnett, R.L., Austermann, J., Dyer, B., Telfer, M.W., Barlow, N.L.M., Boulton, S.J., Carr, A.S., Creel, R.C., 2023. Constraining the contribution of the Antarctic Ice sheet to Last Interglacial sea level. Sci. Adv. 9. https://doi.org/10.1126/sciadv.adf0198 eadf0198.

Burdette, K.E., Rink, J.W., Means, G.H., Portell, R.W., 2009. Optical dating of the anastasia formation, northeastern florida, USA. SE. Geol. 46, 173–185.

Burdette, K.E., Rink, W.J., López, G.I., Mallinson, D.J., Parham, P.R., Reinhardt, E.G., 2012. Geological investigation and optical dating of Quaternary siliciclastic sediments near Apalachicola, North-west Florida, USA. Sedimentology 59, 1836–1849. https://doi.org/10.1111/j.1365-3091.2012.01328.x.

Burdette, K.E., Rink, W.J., Mallinson, D.J., Means, G.H., Parham, P.R., 2013. Electron spin resonance optical dating of marine, estuarine, and aeolian sediments in Florida, USA. Quat. Res. 79, 66–74. https://doi.org/10.1016/j.yqres.2012.10.001.

urdette, K.E., Rink, W.J., Mallinson, D.J., Parham, P.R., Reinhardt, E.G., 2010. Geologic investigation and optical dating of the merritt island sand ridge sequence, Eastern Florida, USA. SE. Geol. 47, 175–190, 10B.

Calvin, K., Dasgupta, D., Krinner, G., Mukherji, A., Thorne, P.W., Trisos, C., Romero, J., Aldunce, P., Barrett, K., Blanco, G., Cheung, W.W.L., Connors, S., Denton, F., Diongue-Niang, A., Dodman, D., Garschagen, M., Geden, O., Hayward, B., Jones, C., Jotzo, F., Krug, T., Lasco, R., Lee, Y.-Y., Masson-Delmotte, V., Meinshausen, M., Mintenbeck, K., Mokssit, A., Otto, F.E.L., Pathak, M., Pirani, A., Poloczanska, E., Pörtner, H.-O., Revi, A., Roberts, D.C., Roy, J., Ruane, A.C., Skea, J., Shukla, P.R., Slade, R., Slangen, A., Sokona, Y., Sörensson, A.A., Tignor, M., Van Vuuren, D., Wei, Y.-M., Winkler, H., Zhai, P., Zommers, Z., Hourcade, J.-C., Johnson, F.X., Pachauri, S., Simpson, N.P., Singh, C., Thomas, A., Totin, E., Arias, P., Bustamante, M., Elgizouli, I., Flato, G., Howden, M., Méndez-Vallejo, C., Pereira, J. J., Pichs-Madruga, R., Rose, S.K., Saheb, Y., Sánchez Rodríguez, R., Ürge-Vorsatz, D., Xiao, C., Yassaa, N., Alegría, A., Armour, K., Bednar-Friedl, B., Blok, K., Cissé, G., Dentener, F., Eriksen, S., Fischer, E., Garner, G., Guivarch, C., Haasnoot, M., Hansen, G., Hauser, M., Hawkins, E., Hermans, T., Kopp, R., Leprince-Ringuet, N., Lewis, J., Ley, D., Ludden, C., Niamir, L., Nicholls, Z., Some, S., Szopa, S., Trewin, B., Van Der Wijst, K.-I., Winter, G., Witting, M., Birt, A., Ha, M., Romero, J., Kim, J., Haites, E.F., Jung, Y., Stavins, R., Birt, A., Ha, M., Orendain, D.J.A., Ignon, L., Park, S., Park, Y., Reisinger, A., Cammaramo, D., Fischlin, A., Fuglestvedt, J.S., Hansen, G., Ludden, C., Masson-Delmotte, V., Matthews, J.B.R., Mintenbeck, K., Pirani, A., Poloczanska, E., Leprince-Ringuet, N., Péan, C., 2023. IPCC, 2023: climate change 2023: synthesis Report. In: Lee, H., Romero, J. (Eds.), Contribution of Working Groups I, II and III to the Sixth Assessment Report of the Intergovernmental Panel on Climate Change [Core Writing Team, IPCC. Intergovernmental Panel on Climate Change (IPCC), Geneva, Switzerland. https://doi.org/10.59327/IPCC/AR6-9789291691647.

Cann, J.H., Murray-Wallace, C.V., 2012. Interstadial age (MIS5c) beach-dune barrier deposits in the Coorong Lagoon, South Australia. Aust. J. Earth Sci. 59, 1127–1134. https://doi.org/10.1080/08120099.2012.727869.

Carrere, L., Lyard, F., Cancet, M., Allain, D., Dabat, M.-L., Fouchet, E., Sahuc, E., Faugere, Y., Dibarboure, G., Picot, N., 2022. A new barotropic tide model for global ocean: FES2022. Presented at the 2022 Ocean Surface Topography Science Team Meeting. https://doi.org/10.24400/527896/a03-2022.3287.

Chutcharavan, P.M., Dutton, A., 2021. A global compilation of U-series-dated fossil coral sea-level indicators for the Last Interglacial period (Marine Isotope Stage 5e). Earth Syst. Sci. Data 13, 3155–3178. https://doi.org/10.5194/essd-13-3155-2021.

Creel, R.C., Austermann, J., 2024. Glacial isostatic adjustment driven by asymmetric ice sheet melt during the Last Interglacial causes multiple local sea-level peaks. Geology 53, 253–258. https://doi.org/10.1130/G52483.1.

Creveling, J.R., Austermann, J., Dutton, A., 2019. Uplift of Trail Ridge, Florida, by Karst Dissolution, glacial isostatic adjustment, and dynamic topography. J. Geophys. Res. Solid Earth 124, 13354–13366. https://doi.org/10.1029/2019JB018489.

Creveling, J.R., Mitrovica, J.X., Clark, P.U., Waelbroeck, C., Pico, T., 2017. Predicted bounds on peak global mean sea level during marine isotope stages 5a and 5c. Quat. Sci. Rev. 163, 193–208. https://doi.org/10.1016/j.quascirev.2017.03.003.

Cronin, T.M., Bybell, L.M., Poore, R.Z., Blackwelder, B.W., Liddicoat, J.C., Hazel, J.E., 1984. Age and correlation of emerged pliocene and pleistocene deposits, U.S. Atlantic Coastal Plain. Palaeogeography, Palaeoclimatology, Palaeoecology, Studies in North American cenozoic correlations 47, 21–51. https://doi.org/10.1016/0031-0182(84)90079-8.

Cronin, T.M., Szabo, B.J., Ager, T.A., Hazel, J.E., Owens, J.P., 1981. Quaternary climates and Sea levels of the U.S. Atlantic coastal Plain. Science 211, 233–240. https://doi.org/10.1126/science.211.4479.233.

Dalton, A.S., Finkelstein, S.A., Barnett, P.J., Forman, S.L., 2016. Constraining the Late Pleistocene history of the Laurentide Ice Sheet by dating the Missinaibi Formation, Hudson Bay Lowlands, Canada. Quat. Sci. Rev. 146, 288–299. https://doi.org/10.1016/j.quascirev.2016.06.015.

Dicken, C.L., Nicholson, S.W., Horton, J.D., Foose, M.P., Mueller, J.A., 2005a. Preliminary integrated geologic map databases for the United States: alabama, Florida, Georgia, Mississippi, North Carolina, and South Carolina. US Geological Survey.

Dicken, C.L., Nicholson, S.W., Horton, J.D., Kinney, S.A., Gunther, G.L., Foose, M.P., Mueller, J.A., 2005b. Preliminary Integrated Geologic Map Databases for the United States: Delaware. US Geological Survey, Maryland, New York, Pennsylvania, and Virginia.

Doar III, William Richardson, 2014. Geologic map of the Myrtle beach quadrangle, Horry County, South Carolina. Geological Map. OFR-209. South Carolina Department of Natural Resources Geological Survey 1, 24000. https://ngmdb.usgs.gov/Prodesc/proddesc_103893.htm.

Doar III, William Richardson, 2015. Geologic map of the wampee quadrangle, Horry County, South Carolina. Geological Map. OFR-215. South Carolina Department of Natural Resources Geological Survey 1, 24000. https://ngmdb.usgs.gov/Prodesc/proddesc_103394.htm.

Doar III, W.R., 2020. Pleistocene Highstand Scarps and Terraces.

Doar III, W.R., 2003. Geologic map of the Beaufort quadrangle, Beaufort County, South Carolina. Geologic Quadrangle Map GQM-22.

Doar III, W.R., 2012. The orangeburg and parler scarps: surficial contacts separating the Eocene, Pliocene, and Pleistocene sediments. Allendale, South Carolina. South Carolina Geological Survey.

Doar III, W.R., Kendall, C.G.St.C., 2014. An analysis and comparison of observed Pleistocene South Carolina (USA) shoreline elevations with predicted elevations derived from Marine oxygen isotope stages. Quat. Res. 82, 164–174. https://doi.org/10.1016/j.yqres.2014.04.005.

Doering, J.A., 1960. Quaternary surface formations of Southern part of Atlantic coastal plain. J. Geol. 68, 182–202. https://doi.org/10.1086/626652.

Dorale, J.A., Onac, B.P., Fornós, J.J., Ginés, J., Ginés, A., Tuccimei, P., Peate, D.W., 2010. Sea-level highstand 81,000 years ago in mallorca. Science 327, 860–863. https://doi.org/10.1126/science.1181725.

Doran, K.S., Long, J.W., Birchler, J.J., Brenner, O.T., Hardy, M.W., Morgan, Karen L.M., Stockdon, Hilary F., Torres, Miguel L., 2024. Lidar-derived beach morphology (dune crest, dune toe, and shoreline) for U.S. sandy coastlines. https://doi.org/10.5066/F7GF0S0Z.

Dowsett, H., Cronin, T., 1990. High eustatic sea level during the middle Pliocene: evidence from the southeastern U.S. Atlantic coastal plain. Geology 18, 435. https://doi.org/10.1130/0091-7613(1990)018<0435:HESLDT>2.3.CO;2.

DuBar, J.R., DuBar, S.S., Ward, L.W., Blackwelder, B.W., Abbot, W.H., Huddleston, P.F., Frey, R.W., 1980. Cenozoic biostratigraphy of the carolina outer coastal plain. Excursions in southeastern geology 1, 179–236.

DuBar, J.R., Johnson, H.S., Thom, B., Hatchell, W.O., 1974. Neogene stratigraphy and morphology, south flank of the Cape Fear Arch, North and South Carolina. In: Oaks, R.Q., DuBar, J.R. (Eds.), Post-Miocene Stratigraphy, Central and Southern Atlantic Coastal Plain. Utah State University Press, pp. 139–173.

Dumitru, O.A., Dyer, B., Austermann, J., Sandstrom, M.R., Goldstein, S.L., D'Andrea, W. J., Cashman, M., Creel, R., Bolge, L., Raymo, M.E., 2023. Last interglacial global mean sea level from high-precision U-series ages of Bahamian fossil coral reefs. Quat. Sci. Rev. 318, 108287. https://doi.org/10.1016/j.quascirev.2023.108287.

Durcan, J.A., King, G.E., Duller, G.A., 2015. DRAC: Dose rate and age calculator for trapped charge dating. Quat. Geochronol. 28, 54–61.

Dutton, A., Carlson, A.E., Long, A.J., Milne, G.A., Clark, P.U., DeConto, R., Horton, B.P., Rahmstorf, S., Raymo, M.E., 2015. Sea-level rise due to polar ice-sheet mass loss during past warm periods. Science 349. https://doi.org/10.1126/science.aaa4019 aaa4019.

Dutton, A., Lambeck, K., 2012. Ice volume and sea level during the last interglacial. Science 337, 216–219. https://doi.org/10.1126/science.1205749.

Dyer, B., Austermann, J., D'Andrea, W.J., Creel, R.C., Sandstrom, M.R., Cashman, M., Rovere, A., Raymo, M.E., 2021. Sea-level trends across The Bahamas constrain peak last interglacial ice melt. Proc. Natl. Acad. Sci. 118, e2026839118. https://doi.org/10.1073/pnas.2026839118.

Emlid, 2025. Glossary | Emlid Studio [WWW Document]. Glossary | Emlid Studio. URL. https://docs.emlid.com/emlid-studio/reference/glossary/, 3.5.25.

Engelhart, S.E., Horton, B.P., 2012. Holocene sea level database for the Atlantic coast of the United States. Quaternary science reviews. Coastal Change during the Late Quaternary 54, 12–25. https://doi.org/10.1016/j.quascirev.2011.09.013.

Engelhart, S.E., Horton, B.P., Kemp, A.C., 2011a. Holocene sea level changes along the United States' Atlantic Coast. Oceanography (Wash. D. C.) 24, 70–79.

Engelhart, S.E., Peltier, W.R., Horton, B.P., 2011b. Holocene relative sea-level changes and glacial isostatic adjustment of the U.S. Atlantic coast. Geology 39 (1), 751–754. https://doi.org/10.1130/G31857.

Flint, S., Aitken, J., Hampson, G., 1995. Application of sequence stratigraphy to coal-bearing coastal plain successions. implications for the UK Coal Measures. SP 82, 1–16. https://doi.org/10.1144/GSL.SP.1995.082.01.01.

Freisleben, R., Jara-Muñoz, J., Melnick, D., Martínez, J.M., Strecker, M.R., 2021. Marine terraces of the last interglacial period along the Pacific coast of South America (1°N–40°S). Earth Syst. Sci. Data 13, 2487–2513. https://doi.org/10.5194/essd-13-2487-2021.

Galbraith, R.F., Roberts, R.G., Laslett, G.M., Yoshida, H., Olley, J.M., 1999. Optical dating of single and multiple grains of quartz from JINMIUM rock shelter, northern Australia: part I, experimental design and statistical models. Archaeometry 41, 339–364. https://doi.org/10.1111/j.1475-4754.1999.tb00987.x.

Guérin, G., Mercier, N., Adamiec, G., 2011. Dose-rate conversion factors: update. Ancient TL 29, 5–8. https://doi.org/10.26034/la.atl.2011.443.

Hibbert, F.D., Rohling, E.J., Dutton, A., Williams, F.H., Chutcharavan, P.M., Zhao, C., Tamisiea, M.E., 2016. Coral indicators of past sea-level change: a global repository of U-series dated benchmarks. Quat. Sci. Rev. 145, 1–56. https://doi.org/10.1016/j.quascirev.2016.04.019.

Hollin, J.T., Hearty, P.J., 1990. South Carolina interglacial sites and stage 5 sea levels. Quat. Res. 33, 1–17.

Hollyday, A., Raymo, M.E., Austermann, J., Richards, F., Hoggard, M., Rovere, A., 2024. Pliocene shorelines and the epeirogenic motion of continental margins: a target dataset for dynamic topography models. Earth Surf. Dyn. 12, 883–905. https://doi.org/10.5194/esurf-12-883-2024.

Horton, B.P., Edwards, R.J., 2005. The application of local and regional transfer functions to the reconstruction of Holocene sea levels, north Norfolk, England. Holocene 15, 216–228. https://doi.org/10.1191/0959683605hl787rp.

Hoyt, J.H., 1969. Late Cenozoic structural movement, Northern Florida1: abstract. AAPG (Am. Assoc. Pet. Geol.) Bull. 53, 2038. https://doi.org/10.1306/5D25C8DB-16C1-11D7-8645000102C1865D.

Hsia, S., Toth, L.T., Mortlock, R., Kerans, C., 2024. Re-evaluating marine isotope stage 5a paleo-sea-level trends from across the Florida keys reef tract. Quaternary Science Advances 15, 100222. https://doi.org/10.1016/j.qsa.2024.100222.

IPCC, 2015. Climate Change 2014: Synthesis Report (IPCC AR5). Intergovernmental Panel on Climate Change, Geneva, Switzerland.

Karegar, M.A., Dixon, T.H., Engelhart, S.E., 2016. Subsidence along the Atlantic Coast of North America: insights from GPS and late Holocene relative sea level data. Geophys. Res. Lett. 43, 3126–3133. https://doi.org/10.1002/2016GL068015.

Khan, N.S., Horton, B.P., Engelhart, S., Rovere, A., Vacchi, M., Ashe, E.L., Törnqvist, T.E., Dutton, A., Hijma, M.P., Shennan, I., 2019. Inception of a global atlas of sea levels since the last glacial maximum. Quat. Sci. Rev. 220, 359–371. https://doi.org/10.1016/j.quascirev.2019.07.016.

Kopp, R.E., Simons, F.J., Mitrovica, J.X., Maloof, A.C., Oppenheimer, M., 2009. Probabilistic assessment of sea level during the last interglacial stage. Nature 462, 863–867. https://doi.org/10.1038/nature08686.

Kreutzer, S., Schmidt, C., DeWitt, R., Fuchs, M., 2014. The a-value of polymineral fine grain samples measured with the post-IR IRSL protocol. Radiat. Meas. 69, 18–29.

Kuchar, J., Milne, G., Latychev, K., 2019. The importance of lateral Earth structure for North American glacial isostatic adjustment. Earth Planet Sci. Lett. 512, 236–245. https://doi.org/10.1016/j.epsl.2019.01.046.

Lambeck, K., Chappell, J., 2001. Sea level change through the last glacial cycle. Science 292, 679–686. https://doi.org/10.1126/science.1059549.

Lamothe, M., 2016. Luminescence dating of interglacial coastal depositional systems: recent developments and future avenues of research. Quat. Sci. Rev. 146, 1–27. https://doi.org/10.1016/j.quascirev.2016.05.005.

Law-Chune, S., Aouf, L., Dalphinet, A., Levier, B., Drillet, Y., Drevillon, M., 2021. WAVERYS: a CMEMS global wave reanalysis during the altimetry period. Ocean Dyn. 71, 357–378. https://doi.org/10.1007/s10236-020-01433-w.

Lee, K.-H., Mizutani, N., 2010. Experimental study of wave breaking of periodic waves on a gravel beach. coas 2010 967–975. https://doi.org/10.2112/JCOASTRES-D-10-00039.1.

Lorscheid, T., Rovere, A., 2019. The indicative meaning calculator – quantification of paleo sea-level relationships by using global wave and tide datasets. Open geospatial data, softw. stand. 4, 10. https://doi.org/10.1186/s40965-019-0069-8.

Mallinson, D., Burdette, K., Mahan, S., Brook, G., 2008. Optically stimulated luminescence age controls on late Pleistocene and Holocene coastal lithosomes, North Carolina, USA. Quat. Res. 69, 97–109. https://doi.org/10.1016/j.yqres.2007.10.002.

Marple, R., Talwani, P., 2004. Proposed Shenandoah fault and East-Coast Stafford fault system and their implications for Eastern US tectonics. SE. Geol. 43, 57–80.

Marple, R.T., Talwani, P., 2000. Evidence for a buried fault system in the coastal plain of the Carolinas and Virginia—implications for neotectonics in the southeastern United States. GSA Bulletin 112, 200–220. https://doi.org/10.1130/0016-7606(2000)112<200:EFABFS>2.0.CO;2.

McCartan, L., Owens, J.P., Blackwelder, B.W., Szabo, B.J., Belknap, D.F., Kriausakul, N., Mitterer, R.M., Wehmiller, J.F., 1982. Comparison of amino acid racemization geochronometry with lithostratigraphy, biostratigraphy, uranium-series coral dating, and magnetostratigraphy in the Atlantic coastal plain of the southeastern United States. Quat. Res. 18, 337–359. https://doi.org/10.1016/0033-5894(82)90078-3.

Mitrovica, J.X., Austermann, J., Coulson, S., Creveling, J.R., Hoggard, M.J., Jarvis, G.T., Richards, F.D., 2020. Dynamic topography and ice age paleoclimate. Annu. Rev. Earth Planet Sci. 48, 585–621. https://doi.org/10.1146/annurev-earth-082517-010225.

Mitrovica, J.X., Milne, G.A., 2003. On post-glacial sea level: I. General theory. Geophys. J. Int. 154, 253–267.

Moucha, R., Ruetenik, G.A., 2017. Interplay between dynamic topography and flexure along the U.S. Atlantic passive margin: insights from landscape evolution modeling. Global Planet. Change 149, 72–78. https://doi.org/10.1016/j.gloplacha.2017.01.004.

Muhs, D.R., Simmons, K.R., Schumann, R.R., Halley, R.B., 2011. Sea-level history of the past two interglacial periods: new evidence from U-series dating of reef corals from south Florida. Quat. Sci. Rev. 30, 570–590. https://doi.org/10.1016/j.quascirev.2010.12.019.

Muhs, D.R., Wehmiller, J.F., Simmons, K.R., York, L.L., 2003. Quaternary sea-level history of the United States. In: Developments in Quaternary Sciences, the Quaternary Period in the United States. Elsevier, pp. 147–183. https://doi.org/10.1016/S1571-0866(03)01008-X.

Multer, H.G., Gischler, E., Lundberg, J., Simmons, K.R., Shinn, E.A., 2002. Key largo limestone revisited: pleistocene shelf-edge facies, Florida keys, USA. Facies 46, 229–271. https://doi.org/10.1007/BF02668083.

Murray, A.S., Wintle, A.G., 2000. Luminescence dating of quartz using an improved single-aliquot regenerative-dose protocol. Radiat. Meas. 32, 57–73.

NGS, 2024. SCHY official station page [WWW Document]. URL. https://geodesy.noaa.gov/CORS/ncn_station_pages/index.html?stationID=SCHY, 5.23.25.

NOAA, 2025. Datums for 8661070, Springmaid Pier SC [WWW Document]. NOAA Tides & Currents. URL. https://tidesandcurrents.noaa.gov/datums.html?datum=MSL&units=1&epoch=0&id=8661070&name=Springmaid+Pier&state=SC, 3.3.25.

NOAA, 2023. Coastal relief models (CRMs). https://doi.org/10.25921/5ZN5-KN44.

Ohenhen, L.O., Shirzaei, M., Ojha, C., Kirwan, M.L., 2023. Hidden vulnerability of US Atlantic coast to sea-level rise due to vertical land motion. Nat. Commun. 14, 2038. https://doi.org/10.1038/s41467-023-37853-7.

Parham, P.R., Riggs, S.R., Culver, S.J., Mallinson, D.J., Jack Rink, W., Burdette, K., 2013. Quaternary coastal lithofacies, sequence development and stratigraphy in a passive margin setting, North Carolina and Virginia, USA. Sedimentology 60, 503–547. https://doi.org/10.1111/j.1365-3091.2012.01349.x.

Peltier, W.R., Argus, D.F., Drummond, R., 2015. Space geodesy constrains ice age terminal deglaciation: the global ICE-6G_C (VM5a) model. J. Geophys. Res. Solid Earth 120, 450–487. https://doi.org/10.1002/2014JB011176.

Peters, S.E., McClennen, M., 2016. The Paleobiology database application programming interface. Paleobiology 42, 1–7. https://doi.org/10.1017/pab.2015.39.

Pico, T., 2020. Towards assessing the influence of sediment loading on Last Interglacial sea level. Geophys. J. Int. 220, 384–392. https://doi.org/10.1093/gji/ggz447.

Pico, T., Creveling, J.R., Mitrovica, J.X., 2017. Sea-level records from the U.S. mid-Atlantic constrain Laurentide ice sheet extent during Marine Isotope Stage 3. Nat. Commun. 8, 15612. https://doi.org/10.1038/ncomms15612.

Poirier, R., Cronin, T., Katz, M.E., Schaller, M.F., Miller, K.G., Miller, K.G., Browning, J. V., McCoy, K.J., Toomey, M., Willard, D., 2021. Paper No. 139-7: Multi-Proxy Constraints on Marine Isotope Stage 5e Sea-Level Position in the U.s. Atlantic Coastal Plain: Implications for Glacio-Isostatic Adjustment and Sea-Level Modeling. GSA 2021. Presented at the GSA Connects 2021. GSA, Portland, Oregon. https://doi.org/10.1130/abs/2021AM-368190.

Potter, E.-K., Esat, T.M., Schellmann, G., Radtke, U., Lambeck, K., McCulloch, M.T., 2004. Suborbital-period sea-level oscillations during marine isotope substages 5a and 5c. Earth Planet Sci. Lett. 225, 191–204. https://doi.org/10.1016/j.epsl.2004.05.034.

Prescott, J.R., Hutton, J.T., 1994. Cosmic ray contributions to dose rates for luminescence and ESR dating: large depths and long-term time variations. Radiat. Meas. 23, 497–500.

Ramsey, K.W., Tomlinson, J.L., Mattheus, C.R., 2022. A radiocarbon chronology of Holocene climate change and sea-level rise at the delmarva peninsula, US Mid-Atlantic Coast. Holocene 32, 3–16. https://doi.org/10.1177/09596836211048282.

Riedesel, S., Burow, C., Kreutzer aut, S., Burow, Christoph, Dietze, M., Fuchs, M.C., Schmidt, C., Fischer, M., Friedrich, J., Mercier, N., Smedley, R.K., Christophe, C., Zink, A., Durcan, J., King, G.E., Philippe, A., Guérin, G., Riedesel, Svenja, Autzen, M., Guibert, P., Mittelstrass, D., Gray, H.J., Galharret, J.-M., Colombo, M., Steinbuch, L., Boer, A.-M. de, Fuchs, M., 2022. scale_GammaDose(.): calculate the gamma dose deposited within a sample taking layer-to-layer variations in radioactivity into account (according to Aitken, 1985). From Package Luminescence: Comprehensive Luminescence Dating Data Analysis.

Rohling, E.J., Hibbert, F.D., Grant, K.M., Galaasen, E.V., Irvalı, N., Kleiven, H.F., Marino, G., Ninnemann, U., Roberts, A.P., Rosenthal, Y., Schulz, H., Williams, F.H., Yu, J., 2019. Asynchronous Antarctic and Greenland ice-volume contributions to the last interglacial sea-level highstand. Nat. Commun. 10, 5040. https://doi.org/10.1038/s41467-019-12874-3.

Rovere, A., Hearty, P.J., Austermann, J., Mitrovica, J.X., Gale, J., Moucha, R., Forte, A. M., Raymo, M.E., 2015. Mid-Pliocene shorelines of the US Atlantic coastal plain — an improved elevation database with comparison to Earth model predictions. Earth Sci. Rev. 145, 117–131. https://doi.org/10.1016/j.earscirev.2015.02.007.

Rovere, A., Pappalardo, M., Richiano, S., Ryan, D.D., Rubio-Sandoval, K., Ruiz, P.M., Montes, A., Gowan, E.J., 2025. Reconstructing past sea-level changes from storm-built beach ridges. Geomorphology 476, 109659. https://doi.org/10.1016/j.geomorph.2025.109659.

Rovere, A., Pico, T., Richards, F., O'Leary, M.J., Mitrovica, J.X., Goodwin, I.D., Austermann, J., Latychev, K., 2023. Influence of reef isostasy, dynamic topography, and glacial isostatic adjustment on sea-level records in Northeastern Australia. Commun. Earth Environ. 4, 1–12. https://doi.org/10.1038/s43247-023-00967-3.

Rovere, A., Raymo, M.E., Vacchi, M., Lorscheid, T., Stocchi, P., Gómez-Pujol, L., Harris, D.L., Casella, E., O'Leary, M.J., Hearty, P.J., 2016a. The analysis of Last Interglacial (MIS 5e) relative sea-level indicators: reconstructing sea-level in a warmer world. Earth Sci. Rev. 159, 404–427. https://doi.org/10.1016/j.earscirev.2016.06.006.

Rovere, A., Ryan, D.D., Vacchi, M., Dutton, A., Simms, A.R., Murray-Wallace, C.V., 2022. The World Atlas of Last Interglacial Shorelines (version 1.0). Earth Syst. Sci. Data Discuss. 1–37. https://doi.org/10.5194/essd-2022-198.

Rovere, A., Stocchi, P., Vacchi, M., 2016b. Eustatic and relative sea level changes. Curr. Clim. Change Rep. 2, 221–231. https://doi.org/10.1007/s40641-016-0045-7.

Rowe, M.P., Wainer, K.A.I., Bristow, C.S., Thomas, A.L., 2014. Anomalous MIS 7 sea level recorded on Bermuda. Quat. Sci. Rev. 90, 47–59. https://doi.org/10.1016/j.quascirev.2014.02.012.

Rowley, D.B., Forte, A.M., Moucha, R., Mitrovica, J.X., Simmons, N.A., Grand, S.P., 2013. Dynamic topography change of the Eastern United States since 3 million years ago. Science 340, 1560–1563. https://doi.org/10.1126/science.1229180.

Roy, K., Peltier, W.R., 2015. Glacial isostatic adjustment, relative sea level history and mantle viscosity: reconciling relative sea level model predictions for the U.S. East coast with geological constraints. Geophys. J. Int. 201, 1156–1181. https://doi.org/10.1093/gji/ggv066.

Ryan, W.B.F., Carbotte, S.M., Coplan, J.O., O'Hara, S., Melkonian, A., Arko, R., Weissel, R.A., Ferrini, V., Goodwillie, A., Nitsche, F., Bonczkowski, J., Zemsky, R., 2009. Global multi-resolution topography synthesis. G-cubed 10. https://doi.org/10.1029/2008GC002332.

Schwab, W.C., Gayes, P.T., Morton, R.A., Driscoll, N.W., Baldwin, W.E., Barnhardt, W.A., Denny, J.F., Harris, M.S., Katuna, M.P., Putney, T.R., 2009. Coastal Change Along the Shore of Northeastern South Carolina-The South Carolina Coastal Erosion Study.

Scott, T.W., Swift, D.J.P., Whittecar, G.R., Brook, G.A., 2010. Glacioisostatic influences on Virginia's late Pleistocene coastal plain deposits. Geomorphology 116, 175–188. https://doi.org/10.1016/j.geomorph.2009.10.017.

Shennan, I., 1986. Flandrian sea-level changes in the Fenland. II: tendencies of sea-level movement, altitudinal changes, and local and regional factors. J. Quat. Sci. 1, 155–179. https://doi.org/10.1002/jqs.3390010205.

Shennan, I., Long, A.J., Horton, B.P. (Eds.), 2015. Handbook of Sea-Level Research. John Wiley & Sons, Ltd, Chichester, UK.

Siddall, M., Chappell, J., Potter, E.-K., 2007. 7. Eustatic sea level during past interglacials. In: Sirocko, F., Claussen, M., Sánchez Goñi, M.F., Litt, T. (Eds.), Developments in Quaternary Sciences, the Climate of past Interglacials. Elsevier, pp. 75–92. https://doi.org/10.1016/S1571-0866(07)80032-7.

Simms, A.R., Anderson, J.B., DeWitt, R., Lambeck, K., Purcell, A., 2013. Quantifying rates of coastal subsidence since the last interglacial and the role of sediment loading. Global Planet. Change 111, 296–308. https://doi.org/10.1016/j.gloplacha.2013.10.002.

Smedley, R.K., Duller, G.A., Pearce, N.J., Roberts, H.M., 2012. Determining the K-content of single-grains of feldspar for luminescence dating. Radiat. Meas. 47, 790–796.

Soller, D.R., 1988. Geology and tectonic history of the lower Cape Fear River Valley, Southeastern North Carolina. Department of the Interior, U.S. Geological Survey.

Szabo, B.J., 1985. Uranium-series dating of fossil corals from marine sediments of southeastern United States Atlantic Coastal Plain. GSA Bulletin 96, 398–406. https://doi.org/10.1130/0016-7606(1985)96<398:UDOFCF>2.0.CO;2.

Tamura, T., 2012. Beach ridges and prograded beach deposits as palaeoenvironment records. Earth Sci. Rev. 114, 279–297. https://doi.org/10.1016/j.earscirev.2012.06.004.

Tawil-Morsink, K., Austermann, J., Dyer, B., Dumitru, O.A., Precht, W.F., Cashman, M., Goldstein, S.L., Raymo, M.E., 2022. Probabilistic investigation of global mean sea level during MIS 5a based on observations from Cave Hill, Barbados. Quat. Sci. Rev. 295, 107783. https://doi.org/10.1016/j.quascirev.2022.107783.

Thiel, C., Buylaert, J.-P., Murray, A., Terhorst, B., Hofer, I., Tsukamoto, S., Frechen, M., 2011. Luminescence dating of the Stratzing loess profile (Austria)–Testing the potential of an elevated temperature post-IR IRSL protocol. Quat. Int. 234, 23–31.

Thompson, S.B., Creveling, J.R., 2021. A global database of marine isotope substage 5a and 5c marine terraces and paleoshoreline indicators. Earth Syst. Sci. Data 13, 3467–3490. https://doi.org/10.5194/essd-13-3467-2021.

Thompson, S.B., Creveling, J.R., Latychev, K., Mitrovica, J.X., 2023. Three-dimensional glacial isostatic adjustment modeling reconciles conflicting geographic trends in North American marine isotope stage 5a relative sea level observations. Geology 51, 808–812. https://doi.org/10.1130/G51257.1.

USGS, 2024. 1/3rd arc-second Digital Elevation Models (Dems) - USGS National Map 3DEP Downloadable Data Collection.

Van De Plassche, O., Wright, A.J., Horton, B.P., Engelhart, S.E., Kemp, A.C., Mallinson, D., Kopp, R.E., 2014. Estimating tectonic uplift of the Cape Fear Arch (south-eastern United States) using reconstructions of Holocene relative sea level. J. Quat. Sci. 29, 749–759. https://doi.org/10.1002/jqs.2746.

Waelbroeck, C., Labeyrie, L., Michel, E., Duplessy, J.C., McManus, J.F., Lambeck, K., Balbon, E., Labracherie, M., 2002. Sea-level and deep water temperature changes derived from benthic Foraminifera isotopic records. Quat. Sci. Rev. 21, 295–305.

Weems, R.E., Lewis Jr., W.M., Lemon Jr., E.M., 2014. Surficial geologic map of the Charleston region. Berkeley, Charleston, Colleton, Dorchester, and Georgetown Counties, South Carolina. Open-File Report, Open-File Report. https://doi.org/10.3133/ofr20131030.

Wehmiller, J.F., 2013. United States Quaternary coastal sequences and molluscan racemization geochronology – what have they meant for each other over the past 45 years? Quaternary Geochronology. Amino Acid Racemization 16, 3–20. https://doi.org/10.1016/j.quageo.2012.05.008.

Wehmiller, J.F., Belknap, D.F., Boutin, B.S., Mirecki, J.E., Rahaim, S.D., York, L.L., Easterbrook, D.L., 1988. A Review of the Aminostratigraphy of Quaternary Mollusks from United States Atlantic Coastal Plain Sites, 227. Geological Society of America Special Paper, pp. 69–110.

Wehmiller, J.F., Brothers, L.L., Ramsey, K.W., Foster, D.S., Mattheus, C.R., Hein, C.J., Shawler, J.L., 2021. Molluscan aminostratigraphy of the US Mid-Atlantic Quaternary coastal system: implications for onshore-offshore correlation, paleochannel and

barrier island evolution, and local late Quaternary sea-level history. Quat. Geochronol. 66, 101177. https://doi.org/10.1016/j.quageo.2021.101177.
Wehmiller, J.F., Simmons, K.R., Cheng, H., Lawrence Edwards, R., Martin-McNaughton, J., York, L.L., Krantz, D.E., Shen, C.-C., 2004. Uranium-series coral ages from the US Atlantic Coastal Plain–the "80 ka problem" revisited. Quaternary International, Coastal Environmental Change during Sea-Level Highstands. IGCP 437 Symposium, Barbados 120, 3–14. https://doi.org/10.1016/j.quaint.2004.01.002.
Wentworth, C.K., 1922. A Scale of grade and class terms for clastic sediments. J. Geol. 30, 377–392.
Willis, R., 2006. Genetic Stratigraphy and Geochronology of Last Interglacial Shorelines on the Central Coast of South Carolina (Master of Science). Louisiana State University and Agricultural and Mechanical College. https://doi.org/10.31390/gradschool_theses.2657.
Winker, C.D., Howard, J.D., 1977a. Correlation of tectonically deformed shorelines on the southern Atlantic coastal plain. Geology 5, 123–127. https://doi.org/10.1130/0091-7613(1977)5<123:COTDSO>2.0.CO;2.
Winker, C.D., Howard, J.D., 1977b. Plio-Pleistocene paleogeography of the Florida Gulf Coast interpreted from Relict shorelines (1). Gulf Coast Association of Geological Societies Transactions 27, 409–420.
Wouters, S., Smith, A.D., 2022. StratigrapheR: Integrated Stratigraphy.
Wu, P.-C., Wei, M. Matt, D'Hondt, S., 2022. Subsidence in coastal cities throughout the world observed by InSAR. Geophys. Res. Lett. 49. https://doi.org/10.1029/2022GL098477 e2022GL098477.